Article

Cell Reports

The Innate Immune Receptor NLRX1 Functions as a Tumor Suppressor by Reducing Colon Tumorigenesis and Key Tumor-Promoting Signals

Graphical Abstract

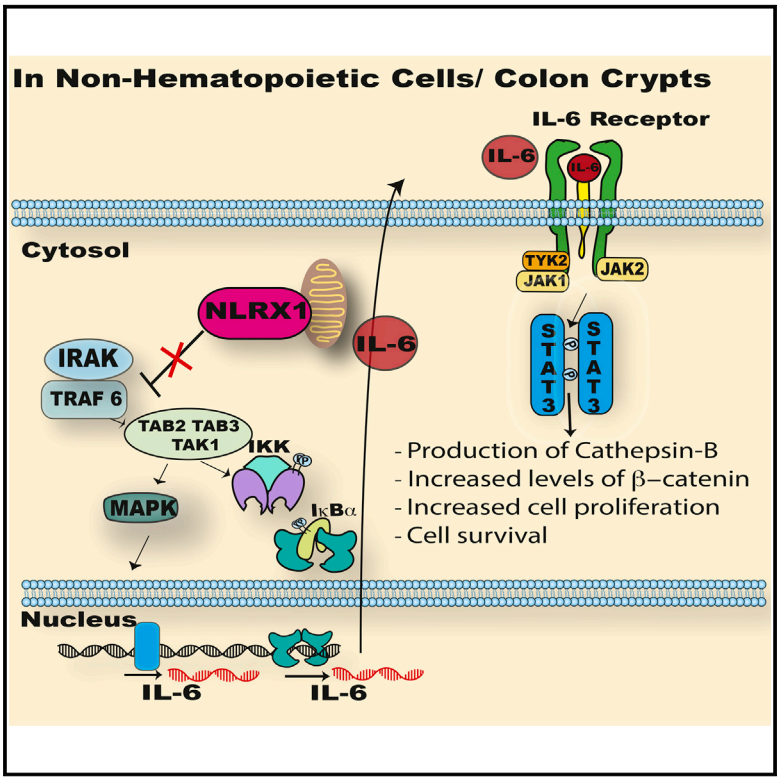

Highlights

- NLRX1 mitigates tumorigenesis in a genetic model of sporadic colon cancer, *APC*$^{min/+}$
- *Nlrx1*$^{-/-}$ colons have increased activation of tumor inducing STAT3, NFκB, MAPK, and IL6
- Anti-IL6R therapy reduces mortality and tumor development in *Nlrx1*$^{-/-}$ *APC*$^{min/+}$ mice
- Human colon tumors exhibit significantly lower levels of NLRX1 in multiple datasets

Authors

A. Alicia Koblansky, Agnieszka D. Truax, Rongrong Liu, ..., Christian Jobin, Pauline Kay Lund, Jenny P.-Y. Ting

Correspondence

jenny_ting@med.unc.edu

In Brief

Koblansky et al. find that loss of NLRX1 increases NF-κB, MAPK, STAT3, and IL-6. Anti-IL6R therapy reduces tumor burden in *Nlrx1*$^{-/-}$*Apc*$^{min/+}$ mice. Human samples reveal that *NLRX1* is lowered in colorectal cancer, indicating its translational importance for understanding colon cancer.

Koblansky et al., 2016, Cell Reports *14*, 1–14
March 22, 2016
http://dx.doi.org/10.1016/j.celrep.2016.02.064

CellPress

Please cite this article in press as: Koblansky et al., The Innate Immune Receptor NLRX1 Functions as a Tumor Suppressor by Reducing Colon Tumorigenesis and Key Tumor-Promoting Signals, Cell Reports (2016), http://dx.doi.org/10.1016/j.celrep.2016.02.064

Cell Reports
Article

The Innate Immune Receptor NLRX1 Functions as a Tumor Suppressor by Reducing Colon Tumorigenesis and Key Tumor-Promoting Signals

A. Alicia Koblansky,[1,8] Agnieszka D. Truax,[1,8] Rongrong Liu,[1,2,8] Stephanie A. Montgomery,[1,3] Shengli Ding,[4] Justin E. Wilson,[1,7] W. June Brickey,[1] Marcus Mühlbauer,[5] Rita-Marie T. McFadden,[1] Peizhen Hu,[6] Zengshan Li,[6] Christian Jobin,[5] Pauline Kay Lund,[4] and Jenny P.-Y. Ting[1,7,*]

[1]The Lineberger Comprehensive Cancer Center, University of North Carolina, Chapel Hill, NC 27599-7295, USA
[2]Department of Microbiology, School of Basic Medicine, Fourth Military Medical University, Xi'an 710032, China
[3]Department of Pathology and Laboratory Medicine, University of North Carolina, Chapel Hill, NC 27599-7295, USA
[4]Department of Cell Biology and Physiology, University of North Carolina, Chapel Hill, NC 27599-7295, USA
[5]Department of Medicine, Division of Gastroenterology, University of Florida College of Medicine, Gainesville, FL 32611, USA
[6]Department of Pathology, Xijing Hospital, Fourth Military Medical University, Xi'an 710032, China
[7]Department of Genetics, University of North Carolina, Chapel Hill, NC 27599-7295, USA
[8]Co-first author
*Correspondence: jenny_ting@med.unc.edu
http://dx.doi.org/10.1016/j.celrep.2016.02.064

SUMMARY

NOD-like receptor (NLR) proteins are intracellular innate immune sensors/receptors that regulate immunity. This work shows that NLRX1 serves as a tumor suppressor in colitis-associated cancer (CAC) and sporadic colon cancer by keeping key tumor promoting pathways in check. *Nlrx1*$^{-/-}$ mice were highly susceptible to CAC, showing increases in key cancer-promoting pathways including nuclear factor κB (NF-κB), mitogen-activated protein kinase (MAPK), signal transducer and activator of transcription 3 (STAT3), and interleukin 6 (IL-6). The tumor-suppressive function of NLRX1 originated primarily from the non-hematopoietic compartment. This prompted an analysis of NLRX1 function in the *Apc*$^{min/+}$ genetic model of sporadic gastrointestinal cancer. NLRX1 attenuated *Apc*$^{min/+}$ colon tumorigenesis, cellular proliferation, NF-κB, MAPK, STAT3 activation, and IL-6 levels. Application of anti-interleukin 6 receptor (IL6R) antibody therapy reduced tumor burden, increased survival, and reduced STAT3 activation in *Nlrx1*$^{-/-}$*Apc*$^{min/+}$ mice. As an important clinical correlate, human colon cancer samples expressed lower levels of *NLRX1* than healthy controls in multiple patient cohorts. These data implicate anti-IL6R as a potential personalized therapy for colon cancers with reduced NLRX1.

INTRODUCTION

Members of the nucleotide binding domain and leucine-rich repeat-containing (NLR, also known as NOD-like receptor) family are evolutionarily conserved components of the immune system that are key mediators of immune defense and inflammation (Takeuchi and Akira, 2010). The major focus in the NLR field is on the inflammasome NLRs, which activate caspase-1 resulting in production of interleukin 1β (IL-1β) and interleukin 18 (IL-18). A subgroup of NLRs play an important role in the regulation of signaling pathways crucial for cell proliferation, survival, cellular differentiation, adhesion, migration, and metabolism, such as mitogen-activated protein kinases (MAPK) and nuclear factor κB (NF-κB) (Hayden and Ghosh, 2011; Sebolt-Leopold and Herrera, 2004; Wullaert et al., 2011). Aberrant activation of these pathways initiate and promote tumor development (Elinav et al., 2013); thus, it is important to determine if NLRs control these pathways during tumorigenesis and if these findings have translational relevance in human cancers.

Colorectal cancer (CRC) is the third most common cancer in both men and women and the second leading cause of cancer-related mortality in the United States with estimates of over 130,000 new cases diagnosed and 50,000 deaths in 2013 (Siegel et al., 2013). Recent studies reported an increased frequency of colon cancer in adults younger than 50, with these patients more likely to show an advance stage of the disease (Bailey et al., 2015). Over 90% of CRCs are adenocarcinomas, while rarer forms include neuroendocrine, squamous cell, spindle cell, and undifferentiated carcinomas (Fleming et al., 2012).

Colitis-associated colon cancer (CAC) accounts for 1% of CRC (Yashiro, 2014). The link between chronic inflammation and increased tumorigenesis has been well documented in inflammatory bowel diseases (IBD), including ulcerative colitis (UC), and Crohn's disease (CD) (Rogler, 2014; Terzić et al., 2010). IBD are associated with increased production of pro-inflammatory cytokines, which are associated with the activation of NF-κB, signal transducer and activator of transcription 3 (STAT3), and mitogen-activated protein kinase (MAPK). Each of these pathways contributes to tumor progression in CRC

Please cite this article in press as: Koblansky et al., The Innate Immune Receptor NLRX1 Functions as a Tumor Suppressor by Reducing Colon Tumorigenesis and Key Tumor-Promoting Signals, Cell Reports (2016), http://dx.doi.org/10.1016/j.celrep.2016.02.064

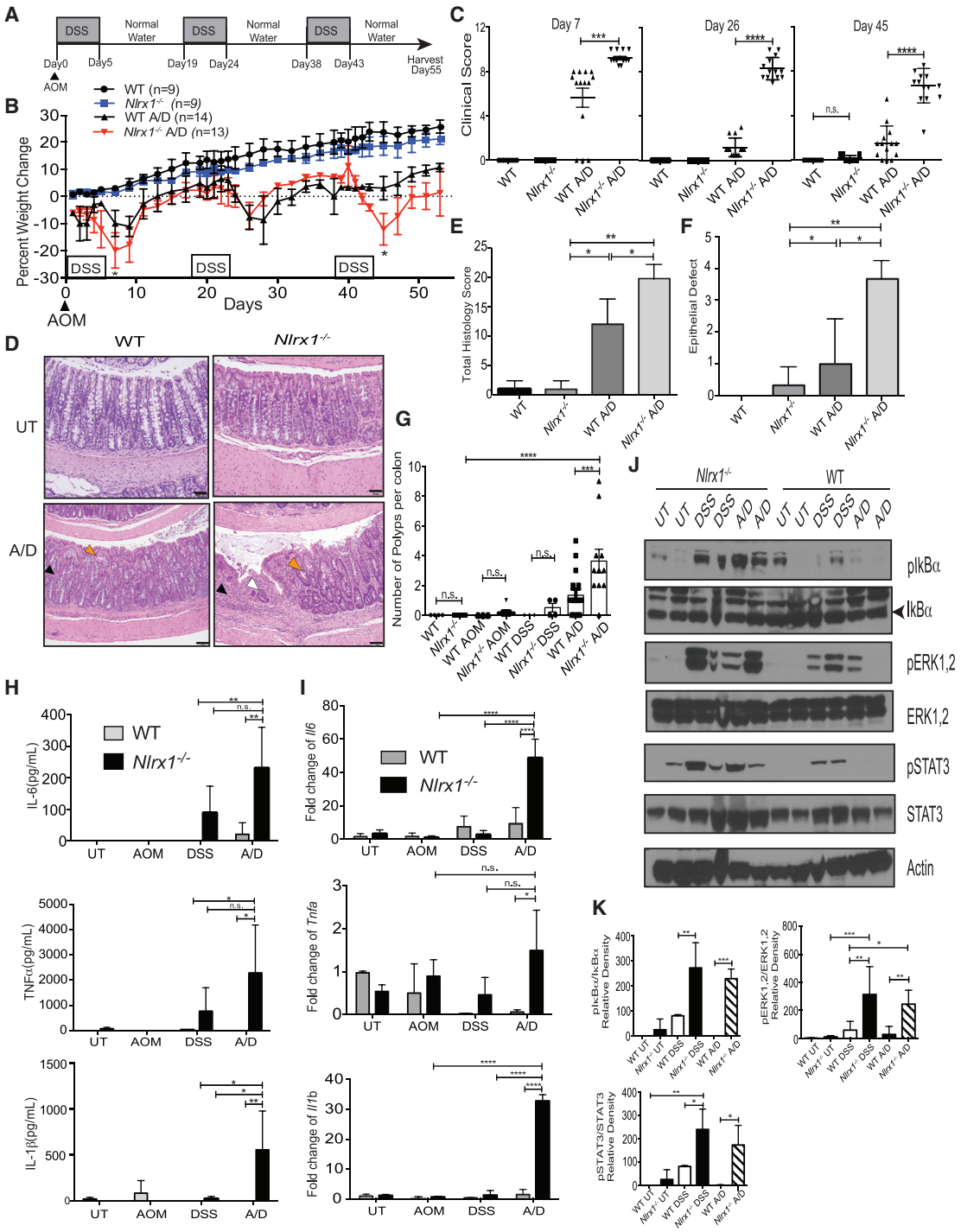

Figure 1. *Nlrx1* Deficiency Leads to Increased Inflammation and Colitis-Associated Tumorigenesis

(A) In the chronic CAC model, WT and *Nlrx1*$^{-/-}$ mice were challenged with A/D.

(B) The percent weight change after A/D treatment is shown. Each data point is the average from three independent experiments with n indicated.

(C) Cumulative clinical scores were measured at days 7, 26, and 45. Each data point represents one animal.

(D) Photomicrographs show H&E-stained colons from untreated (UT) WT, UT *Nlrx1*$^{-/-}$, A/D-treated WT with mild inflammation (black arrowhead) and crypt shortening (white arrowhead), and A/D-treated *Nlrx1*$^{-/-}$ with extensive inflammation (black arrowhead), crypt loss and atrophy (white arrowhead) and early mucosal dysplasia (orange arrowhead). Scale bars represent 50 μm.

(E) Total histology score for UT or A/D-treated WT and *Nlrx1*$^{-/-}$ mice scored in a blinded fashion.

(F) Average epithelial defects were measured from H&E stained colons as indicated. Graph is a compilation of three separate experiments.

(legend continued on next page)

(Ben-Neriah and Karin, 2011; Dhillon et al., 2007; O'Shea et al., 2013). NF-κB regulation of CRC development occurs through the enhanced survival of pre-malignant epithelial cells and release of inflammatory cytokines, which promote tumor growth (Ditsworth and Zong, 2004; Greten et al., 2004; Staudt, 2010). Elevated levels of IL-1β, tumor necrosis factor α (TNF-α), and interleukin 6 (IL-6) are commonly associated with both IBD and CRC (Becker et al., 2005; Lin and Karin, 2007; Waldner et al., 2012). In particular, IL-6 and STAT3 potently stimulate colon cancer proliferation and have critical roles in colon tumor development in preclinical models (Bollrath et al., 2009; Corvinus et al., 2005; Grivennikov et al., 2009). There is also a strong correlation between local IL-6 accumulation and clinical activity of IBD in humans (Atreya and Neurath, 2005; Hyams et al., 1993).

The initial connection between IBD and the NLR family was based on the strong genetic association between NOD2/CARD15 mutations in Crohn's disease and colon cancer (Hugot et al., 2001; Kurzawski et al., 2004; Ogura et al., 2001). Mouse models of CAC have demonstrated that other NLRs, such as NLRP3, NLRP6, and NLRP12, also protect against CAC (Allen et al., 2010; Anand et al., 2012; Chen et al., 2011; Dupaul-Chicoine et al., 2010; Elinav et al., 2011; Zaki et al., 2010). The NLRP3 and NLRP6 inflammasomes appear to limit CAC primarily through the induction of IL-18, while NLRP12 reduces NF-κB and ERK activation, hence reducing chemokines and nitric oxide that promote tumorigenesis (Allen et al., 2012; Zaki et al., 2011).

NLRX1 does not exhibit inflammasome function and is uniquely localized to the mitochondria (Moore et al., 2008; Tattoli et al., 2008). NLRX1 attenuates TRAF6, mitochondrial antiviral signaling protein (MAVS)/retinoic acid-inducible gene I (RIG-I), interferon regulatory factor 3 (IRF3), and IκB kinase (IKK) signaling in response to viral infection and TLR signaling (Allen et al., 2011; Moore et al., 2008; Xia et al., 2011), but it is also required for the induction of reactive oxygen species in response to pathogens (Abdul-Sater et al., 2010; Tattoli et al., 2008). As a result of its impact on key signaling pathways, NLRX1 negatively regulates the expression of pro-inflammatory cytokines, including IL-6 (Allen et al., 2011), a cytokine that has a central role in CAC and is a target of therapies for the treatment of IBD (Allocca et al., 2013). A recent study reported that NLRX1 expression is reduced in patients with chronic obstructive pulmonary disease (COPD), and the absence of NLRX1 exacerbated a model of COPD (Kang et al., 2015). Thus, one of the functions of NLRX1 is to attenuate over-zealous immune responses. Therefore, elucidating the molecular regulation and function of NLRX1 in CAC or sporadic CRC has the potential to identify novel pathways and therapeutic targets for the treatment of colon cancer.

Analyses of inflammasome NLRs in models of CAC have been well reported; however, CAC represents only 1% of CRC. By contrast, the importance of NLRs in the more prevalent sporadic colon tumors is sorely lacking. This current study identifies an important role for *Nlrx1* in suppressing tumorigenesis in both CAC and sporadic colon cancer models by restricting the activation of NF-κB, MAPK, STAT3, and IL-6 production. In contrast to most inflammasome NLRs, which function through the myeloid-monocytic hematopoietic system, NLRX1 exerts its impact primarily through non-hematopoietic cells such as colon crypt cells. The importance of NLRX1 in cells other than hematopoietic is consistent with its role in sporadic CRC modeled after familial adenomatous polyposis (FAP). FAP is a hereditary disease characterized by the development of colon polyps, attributed to the deletion of the *APC* (adenomatous polyposis coli) gene (Fodde et al., 2001). Mutations in the *APC* gene also lead to sporadic colon cancer. The $Apc^{Min/+}$ mouse model has a point mutation in the *Apc* gene, which predisposes the mice to increased spontaneous intestinal polyps. This study reveals that compared to $Apc^{min/+}$ controls, $Apc^{min/+}$ mice lacking *Nlrx1* have a dramatically increased tumor burden accompanied by increased IL-6, STAT3, β-catenin, and cathepsin B activation. Treatment of $Nlrx1^{-/-}Apc^{Min/+}$ mice with anti-IL6R therapy reduced STAT3 activation, decreased tumor number, and increased survival, indicating that increased IL-6 is a causative factor in tumorigenesis linked to NLRX1-deficiency. Expression analyses of clinical human colon cancer samples and meta-analysis of multiple public databases revealed that *NLRX1* expression is significantly lowered in CRC when compared to normal colon tissues. These findings indicate that the loss or reduction of NLRX1 may contribute to human colon cancers.

RESULTS

$Nlrx1^{-/-}$ Mice Are More Susceptible to Chronic Azoxymethane/Dextran Sodium Sulfate-Induced Colitis-Associated Colon Cancer

To test the hypothesis that NLRX1 impacts colon tumorigenesis, $Nlrx1^{-/-}$ and wild-type (WT) littermates were subjected to a well-characterized CAC model that combines the genotoxic DNA-methylation agent, azoxymethane (AOM), and dextran sodium sulfate (DSS) (Neufert et al., 2007). CAC was induced by injecting a single dose of AOM, followed by three cycles of 3% DSS administration for 5 days followed by 14 days of regular drinking water, hereafter referred to as A/D treatment (Figure 1A). A/D-treated $Nlrx1^{-/-}$ mice exhibited statistically greater weight loss than A/D-treated wild-type mice (Figure 1B). A clinical score based on body condition, stool consistency, rectal bleeding,

(G) Quantification of macroscopic polyp formation in the colons of WT and $Nlrx1^{-/-}$ mice after A/D treatment. Each data point represents one animal. Graph is a compilation of three separate experiments.

(H) Serum cytokine levels of IL-6, TNF-α, and IL-1β were measured by ELISA. Values are averages from two independent experiments. $n \geq 6$ mice/group.

(I) Expression of *Il6*, *Tnfα*, and *Il1β* transcript in colon homogenates was measured by qPCR using comparative C_T method ($2^{-\Delta\Delta CT}$) and graphed as fold over UT WT sample (mean ± SEM).

(J) Proteins isolated from distal colonic tissue obtained from UT or A/D-treated WT and $Nlrx1^{-/-}$ mice were analyzed for NF-κB, MAPK, and STAT3 activity by western blot analysis with indicated protein loading control. Each lane represents one animal.

(K) Densitometric measurement of western blots was obtained from three independent experiments. $n \geq 5$ mice/group, n.s., non-significant. *$p < 0.05$, **$p < 0.01$, ***$p < 0.001$, and ****$p < 0.0001$.

See also Figure S1.

Please cite this article in press as: Koblansky et al., The Innate Immune Receptor NLRX1 Functions as a Tumor Suppressor by Reducing Colon Tumorigenesis and Key Tumor-Promoting Signals, Cell Reports (2016), http://dx.doi.org/10.1016/j.celrep.2016.02.064

and the presence of blood in the stool (Allen et al., 2010) was significantly higher in *Nlrx1*$^{-/-}$ animals compared to WT controls (Figure 1C). The histologic appearance of the *Nlrx1*$^{-/-}$ colons harvested at 55 days post A/D injection showed increased total histology score (THS) (Figures 1D and 1E), which evaluates severity and extent of inflammation, epithelial defects, crypt atrophy, and mucosal dysplasia/neoplasia. *Nlrx1*$^{-/-}$-treated colons had more widespread epithelial defects compared to controls as scored in a blinded fashion by a board-certified veterinarian pathologist (Figure 1F, see legend for a detailed description).

On day 55 after the start of A/D, colons were harvested and macroscopic polyps were counted. A/D-treated *Nlrx1*$^{-/-}$ mice exhibited significantly more polyps in the distal region of their colons compared to A/D-treated WT controls (Figure 1G). *Nlrx1*$^{-/-}$ mice also exhibited greater tumor volume compared to WT controls (Figure S1A). Mice treated with DSS or AOM alone had few, if any, polyps. Further analysis by endoscopy with a different group of mice revealed that A/D-treated *Nlrx1*$^{-/-}$ mice developed more polyps or lesions at the time of examination (day 48 of the A/D treatment course) compared to WT control mice (Figure S1B). NLRX1 attenuates cytokine expression in fibroblasts (Allen et al., 2011). To assess if this occurs in CAC, serum from A/D-treated *Nlrx1*$^{-/-}$ mice were prepared and showed significantly higher levels of IL-6, TNF-α, and IL-1β protein than controls as determined by ELISA (Figure 1H) and greater *Il6*, *Tnf*α, and *Il1*β RNA expression as determined by real-time PCR from colon tissues (Figure 1I). Previous reports have demonstrated the role of increased NF-κB and ERK activation in CAC development (Greten et al., 2004). Western blot analysis revealed that colons of chronic DSS- or A/D-treated *Nlrx1*$^{-/-}$ mice had higher levels of phosphorylated IκBα and ERK1/2 compared to WT controls (Figures 1J and 1K). Furthermore, IL-6 induces the activation of STAT3, which is dysregulated in colon cancer. Colons from A/D-treated *Nlrx1*$^{-/-}$ mice had significantly higher levels of phosphorylated STAT3 compared to WT controls (Figures 1J and 1K). These results show that NLRX1 mitigates several known tumor-promoting signaling pathways during CAC.

Nlrx1 Expression in the Non-hematopoietic Compartment Mediates Protection against Colon Tumorigenesis

NLRX1 is widely expressed in different tissues and organs (Moore et al., 2008), hence its impact on CAC might be attributed to its expression in hematopoietic and/or non-hematopoietic cells. To address this, the following four groups of bone marrow chimeras were generated to test whether hematopoietic and/or non-hematopoietic cells were needed to protect against polyp formation: (1) irradiated WT mice that received bone marrow from WT littermates (WT > WT, control group), (2) irradiated WT control mice that received bone marrow from *Nlrx1*$^{-/-}$ donors (*Nlrx1*$^{-/-}$ > WT, hematopoietic component was *Nlrx1*-deficient), (3) irradiated *Nlrx1*$^{-/-}$ mice that received bone marrow from *Nlrx1*$^{-/-}$ donors (*Nlrx1*$^{-/-}$ > *Nlrx1*$^{-/-}$, global *Nlrx1* deficiency), and (4) irradiated *Nlrx1*$^{-/-}$ mice that received bone marrow from WT donors (WT > *Nlrx1*$^{-/-}$, non-hematopoietic compartment was *Nlrx1*-deficient). All reconstituted mice were treated with A/D and monitored for 55 days. Within the first 10–15 days post A/D treatment, almost 50% of the *Nlrx1*$^{-/-}$ > *Nlrx1*$^{-/-}$ and WT > *Nlrx1*$^{-/-}$ mice died (Figure 2A). Of the mice that survived, a clinical score was assessed. WT > *Nlrx1*$^{-/-}$ and *Nlrx1*$^{-/-}$ > *Nlrx1*$^{-/-}$ groups showed increased clinical scores compared to the WT > WT controls and the *Nlrx1*$^{-/-}$ > WT groups at all three indicated time points (Figure 2B). WT > *Nlrx1*$^{-/-}$ and *Nlrx1*$^{-/-}$ > *Nlrx1*$^{-/-}$ groups had an increase in THS when compare to *Nlrx1*$^{-/-}$ > WT group and WT > WT controls (Figures 2C and 2D). *Nlrx1*$^{-/-}$ > *Nlrx1*$^{-/-}$ had a higher THS possibly due to the fact that NRLX1 is expressed in many different cell types (Figure 2D). Similar to findings with non-chimeric *Nlrx1*$^{-/-}$ mice, the *Nlrx1*$^{-/-}$ > *Nlrx1*$^{-/-}$ group had a higher number of colonic polyps than WT > WT controls (Figure 2E). WT > *Nlrx1*$^{-/-}$ mice showed significantly higher numbers of polyps than the WT > WT and *Nlrx1*$^{-/-}$ > WT mice (Figure 2E). Colonic polyp numbers in *Nlrx1*$^{-/-}$ > WT mice were not significantly different from WT > WT controls. *Nlrx1*$^{-/-}$ > *Nlrx1*$^{-/-}$ and *WT* > *Nlrx1*$^{-/-}$ mice, but not *Nlrx1*$^{-/-}$ > WT mice, had significantly increased tumor volume compared to WT > WT mice (Figure 2F). Additionally, phosphorylated STAT3 was higher in *Nlrx1*$^{-/-}$ > *Nlrx1*$^{-/-}$ and *WT* > *Nlrx1*$^{-/-}$ mice compared to *Nlrx1*$^{-/-}$ > WT and WT > WT mice (Figure 2G). A composite of three experiments confirmed these results (Figure 2H). These results indicate that the presence of *Nlrx1* in the non-hematopoietic compartment is primarily required to limit A/D-induced tumorigenesis and STAT3 activation.

Loss of *Nlrx1* in the *Apc*$^{min/+}$ Model of Sporadic CRC Leads to Increased Mortality and Tumor Burden

The above data indicate a contribution of *Nlrx1*-deficiency from the non-hematopoietic compartment during CAC pathogenesis. However, the majority of colon cancers are not associated with CAC. Therefore, we explored the role of NLRX1 in a model of sporadic colon cancer. *APC* mutations are found in ~85% of human colon cancers or precancerous adenomas, and the loss of *APC* in epithelial cells is sufficient to drive intestinal tumorigenesis (Kinzler and Vogelstein, 1996; Schwitalla et al., 2013). *Apc*$^{min/+}$ mice have a germline mutation in the *APC* gene and develop spontaneous polyps (Fodde et al., 2001). Usually, *Apc*$^{min/+}$ mice become moribund within 168 days of age due to complications from intestinal tumors (Heyer et al., 1999). To explore the role of NLRX1 in a model of sporadic colon cancer, *Nlrx1*$^{-/-}$ mice were bred with *Apc*$^{min/+}$ mice to test if the loss of *Nlrx1* affected spontaneous tumor development and lethality. Survival of *Nlrx1*$^{-/-}$*Apc*$^{min/+}$ mice was dramatically decreased when compared to *Apc*$^{min/+}$ littermate controls (Figure 3A). Mice were monitored and harvested at 42, 84, and 168 days of age to elucidate potential factors of early mortality (Figure S2A). At 168 days, *Nlrx1*$^{-/-}$*Apc*$^{min/+}$ mice exhibited obvious signs of hunched back (Figure S2B), which correlated with an increase in clinical score (Figure 3B). *Apc*$^{min/+}$ and *Nlrx1*$^{-/-}$*Apc*$^{min/+}$ mice did not differ in body weight at 84 to 168 days, although there was a slight and statistically significant difference between *Nlrx1*$^{-/-}$ and WT mice at 42 days (Figure S2C). Macroscopic analysis of unstained colons and colons stained by Alcian blue revealed that *Nlrx1*$^{-/-}$*Apc*$^{min/+}$ colons had increased polyps (Figure 3C). The numbers of visible polyps were quantified at three different time points. At 42 days of age, colonic (Figure 3D) polyp

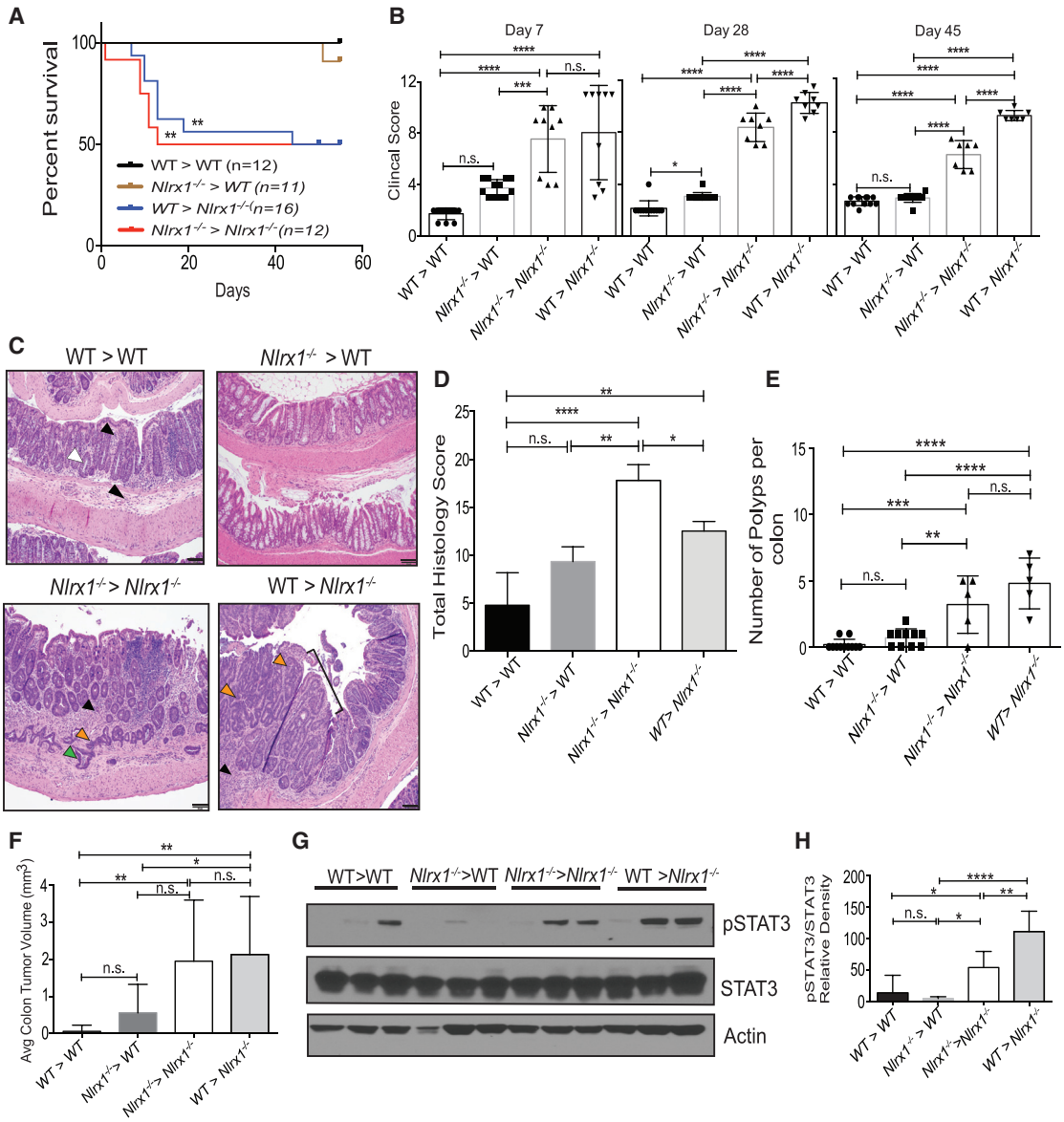

Figure 2. Nlrx1 Expression in the Non-hematopoietic Compartment Is Primarily Required for Protection against AOM/DSS-Induced Tumorigenesis

Bone-marrow chimeras of WT and *Nlrx1*$^{-/-}$ mice were challenged with AOM and 2.5% DSS (A/D).

(A and B) Mice from two independent experiments were monitored for (A) mortality and (B) clinical score of disease; n ≥ 6 mice/group.

(C) Photomicrographs of H&E-stained colons from A/D-treated WT > WT with mucosal and submucosal inflammation (black arrowheads) and crypt shortening (white arrowhead); A/D-treated *Nlrx1*$^{-/-}$ > WT mice with similar features; A/D-treated *Nlrx1*$^{-/-}$ > *Nlrx1*$^{-/-}$ mice with extensive inflammation separating crypts (black arrowhead), crypt dysplasia (orange arrowhead), and partial penetration of muscularis mucosa (green arrowheads); A/D-treated WT > *Nlrx1*$^{-/-}$ mice with inflammation (black arrowhead) and a sessile adenoma (bracket) with dysplasia, including crypt infolding and branching and loss of goblet cells and nuclear polarization (orange arrowheads). Scale bars represent 50 μm.

(D) Total histology score of colons represented in (C).

(E) Macroscopic colonic polyps were counted on day 55 post-A/D treatment. Each data point represents one animal. Graph is the compilation of two independent experiments.

(F) Average colon tumor volume was measured. n ≥ 6 mice/group.

(G) Proteins isolated from distal portion of colons were analyzed by western blot for STAT3 activation. Each lane represents one animal.

(H) Densitometric measurement of western blots was obtained from three independent experiments. n ≥ 5 mice/group, n.s., non-significant. *p < 0.05, **p < 0.01, ***p < 0.001, and ****p < 0.0001.

Please cite this article in press as: Koblansky et al., The Innate Immune Receptor NLRX1 Functions as a Tumor Suppressor by Reducing Colon Tumorigenesis and Key Tumor-Promoting Signals, Cell Reports (2016), http://dx.doi.org/10.1016/j.celrep.2016.02.064

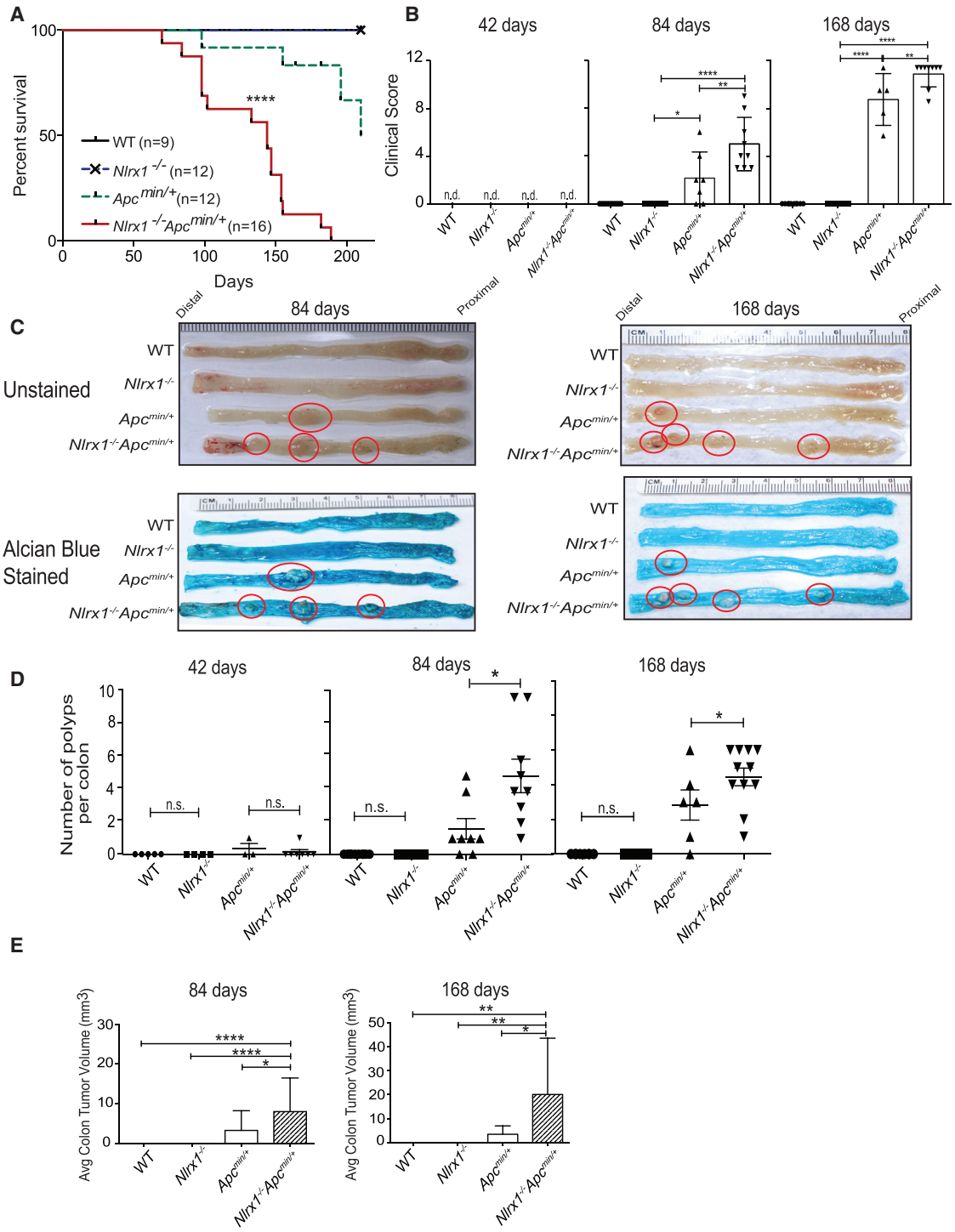

Figure 3. *Nlrx1* Deficiency Leads to Increased Disease and Polyp Burden in the *Apc*$^{min/+}$ Model and Sporadic CRC

(A) WT, *Nlrx1*$^{-/-}$, *Apc*$^{min/+}$, and *Nlrx1*$^{-/-}$*Apc*$^{min/+}$ mice were followed for 168 days for long-term survival; n ≥ 9 mice/group.

(B) Cumulative clinical score of WT, *Nlrx1*$^{-/-}$, *Apc*$^{min/+}$, and *Nlrx1*$^{-/-}$*Apc*$^{min/+}$ mice at 42, 84, and 168 days Images of WT, *Nlrx1*$^{-/-}$, *Apc*$^{min/+}$, and *Nlrx1*$^{-/-}$*Apc*$^{min/+}$ mice at 84 and 168 days of age.

(C) Polyps in representative colons from mice at 84 (left) and 168 days (right) of age that were either unstained (top) or stained with Alcian blue. Polyps are highlighted by red circles.

(D and E) Quantification of macroscopic polyp formation and average tumor volume in the colons of WT, *Nlrx1*$^{-/-}$, *Apc*$^{min/+}$, and *Nlrx1*$^{-/-}$*Apc*$^{min/+}$ mice at 42, 84, and 168 days of age. Each data point represents one animal. n ≥ 5 mice/group, n.s., non-significant. *p < 0.05, **p < 0.01, and ****p < 0.0001.

See also Figure S2.

numbers were not significantly different among the four groups. However, at 84 days and 168 days of age, a modest number of polyps appeared in *Apc*$^{min/+}$ mice as reported in the literature (Heyer et al., 1999), while *Nlrx1*$^{-/-}$*Apc*$^{min/+}$ mice developed significantly more visible polyps in their colons compared to *Apc*$^{min/+}$ mice (Figure 3D). In addition, *Nlrx1*$^{-/-}$*Apc*$^{min/+}$ colons had larger tumor volume when compared to *Apc*$^{min/+}$ colons (Figure 3E). These results suggest that NLRX1 attenuates both polyp number and tumor volume during sporadic colon cancer.

NLRX1 Attenuates Aberrant Cellular Proliferation and Disease Progression in the *APC*$^{min/+}$ Mouse Tumor Model

Histological analysis of H&E-stained colons from 168-day-old *Nlrx1*$^{-/-}$*Apc*$^{min/+}$ mice revealed a higher THS marked by more severe histologic lesions, including increased incidence of colonic dysplasia and neoplasm compared to similar-aged *Apc*$^{min/+}$ or *Nlrx1*$^{-/-}$ mice (Figure 4A, see figure legend for a detailed description of the histology). We also observed a higher rate of distal inflammation in the colons of *Nlrx1*$^{-/-}$*Apc*$^{min/+}$ mice (Figure 4B). In addition, we observed no difference in the percentage of cleaved caspase 3, a marker of apoptosis, between WT and *Nlrx1*$^{-/-}$ (Figure 4C) while we saw significantly higher levels of Ki67^{+} cells in the basal end of colon crypts in *Nlrx1*$^{-/-}$ and *Nlrx1*$^{-/-}$*Apc*$^{min/+}$ mice compared to wild-type and *Apc*$^{min/+}$ mice, which is an indicator of increased proliferation (Figures 4D and 4E). APC controls the stability of β-catenin, a key regulator of Wnt signaling, stem cell renewal, cell fate, and growth (Clevers and Nusse, 2012). Additionally, increased cytoplasmic β-catenin is a marker of carcinogenesis (Fodde et al., 2001). Immunohistochemical staining of *Nlrx1*$^{-/-}$*Apc*$^{min/+}$ tumors showed increased β-catenin compared to *Apc*$^{min/+}$ controls (Figure 4F).

Our findings indicate that STAT3 was hyperactivated in the absence of NLRX1 (Figure 1J). STAT3 is known to activate cathepsin-B, which is involved in the oncogenesis and metastasis of human cancers and it is upregulated in dysplastic adenomas and colorectal carcinoma (Ding et al., 2014; Kuester et al., 2008). Ex vivo imaging of colons of *Nlrx1*$^{-/-}$*Apc*$^{Min/+}$ mice, *Apc*$^{Min/+}$, *Nlrx1*$^{-/-}$, and WT controls injected with a cathepsin B-inducible fluorescence probe (Prosense 680) (Ding et al., 2014; Gounaris et al., 2013) revealed significantly higher fluorescence in colons of *Nlrx1*$^{-/-}$*Apc*$^{Min/+}$ versus *Apc*$^{Min/+}$ mice, which is indicative of increased cathepsin B activity in the *Nlrx1*$^{-/-}$*Apc*$^{Min/+}$ mice (Figure 4G). Colons of *Nlrx1*$^{-/-}$ and WT littermates showed minimal cathepsin B signals (Figure 4G). This result indicates that cathepsin B activity is enhanced in *Nlrx1*$^{-/-}$*Apc*$^{Min/+}$mice.

NLRX1 Attenuates Tumor-Promoting Signaling Pathways in Colon Crypts during the *Apc*$^{min/+}$ Model of Spontaneous CRC

To assess whether the presence of NLRX1 attenuated key tumor-promoting pathways in the *Apc*$^{min/+}$ model, colons were isolated and analyzed by western blot. *Nlrx1*$^{-/-}$*Apc*$^{min/+}$ colons had higher levels of phosphorylated p65, IκBα, JNK1/2, and ERK1/2 at 84 (Figure 5A) and 168 (Figure 5B) days of age compared to *Nlrx1*$^{-/-}$, *Apc*$^{min/+}$, and WT mice. Phosphorylated STAT3 was also elevated in *Nlrx1*$^{-/-}$*Apc*$^{min/+}$ colons (Figures 5A and 5B). Since *Nlrx1*$^{-/-}$*Apc*$^{min/+}$ had increased levels of Ki67^{+} in their colon crypt (Figure 4D), we isolated these cells to determine the impact of NLRX1-deficiency. These cells were EpCAM^{hi} and CD45^{lo} (Figure S3). *Nlrx1*$^{-/-}$*Apc*$^{min/+}$ colon crypts from 84-day-old mice had higher levels of phosphorylated p65, ERK1/2, and STAT3 (Figure 5C) than controls. Since STAT3 can be activated by the key tumor-promoting cytokine, IL-6, *Il6* transcript was measured by qPCR, and it was significantly increased in *Nlrx1*$^{-/-}$*Apc*$^{min/+}$ colons (Figure 5D). In contrast, levels of *Tnfα* and *Il1*β were not significantly different between *Apc*$^{min/+}$ and *Nlrx1*$^{-/-}$*Apc*$^{min/+}$ colons (Figure 5D). ELISA analysis verified significantly higher levels of IL-6 protein produced by colonic samples isolated from *Nlrx1*$^{-/-}$*Apc*$^{min/+}$ animals compared to *Apc*$^{min/+}$ mice, but no difference in IL-1β and TNF-α, which was below detection (Figure 5E). Taken together, these results indicate that the loss of NLRX1-activated multiple pathways that contribute to tumor development or progression.

Anti-IL6R Therapy Significantly Decreases Tumor Burden and STAT3 Activity in the *Nlrx1*$^{-/-}$*Apc*$^{min/+}$ Animals

To assess whether the pathways delineated above contributed to the mechanism by which NLRX1 suppressed tumor growth, we directly assessed the role of elevated IL-6 in *Nlrx1*$^{-/-}$*Apc*$^{min/+}$ animals with antibodies against IL-6 receptor. WT, *Nlrx1*$^{-/-}$, *Apc*$^{min/+}$, and *Nlrx1*$^{-/-}$*Apc*$^{min/+}$ animals were injected with 20 μg/ml of anti-IL6R per mouse biweekly for 10 weeks. Cumulative clinical score revealed that *Nlrx1*$^{-/-}$*Apc*$^{min/+}$ mice on anti-IL6R treatment had a significantly lowered clinical score compared to the untreated (UT) *Nlrx1*$^{-/-}$*Apc*$^{min/+}$ group (Figure 6A). Anti-IL6R-treated *Nlrx1*$^{-/-}$*Apc*$^{min/+}$ mice showed significant weight gain compared to UT controls, while anti-IL6R-treated WT, *Nlrx1*$^{-/-}$, and *Apc*$^{min/+}$showed a modest, but insignificant weight loss compared to their UT controls (Figure 6B). After 10 weeks of anti-IL-6R therapy, colons were harvested and macroscopic polyps were counted. Anti-IL6R-treated *Nlrx1*$^{-/-}$*Apc*$^{min/+}$ animals exhibited significantly less polyps in the distal region of their colons in comparison to UT *Nlrx1*$^{-/-}$*Apc*$^{min/+}$ (Figures 6C and 6D). Western blot showed a significant decrease of phosphorylated STAT3 in anti-IL6R-treated *Nlrx1*$^{-/-}$*Apc*$^{min/+}$ animals in comparison to UT animals (Figure 6E). STAT3 is well documented to regulate the initial events of tumor development, progression, and invasiveness (Waldner et al., 2012) (Figure 6F) and decreased levels of phosphorylated STAT3 observed in anti-IL6R-treated *Nlrx1*$^{-/-}$*Apc*$^{min/+}$ animals correlated positively with decreased polyp numbers (Figures 6D and 6F). Thus, these results indicate that increased IL-6 found in *Nlrx1*$^{-/-}$*Apc*$^{min/+}$ played a causative role in increased polyp formation and heightened STAT3 activation.

NLRX1 Expression Is Reduced in Colorectal Cancer Based on Analysis of the Oncomine Platform and Newly Isolated Clinical Samples

To examine the relevance of the data in preclinical models to human colon cancer, the levels of *NLRX1* expression in human CRC was subjected to bioinformatics mining using the

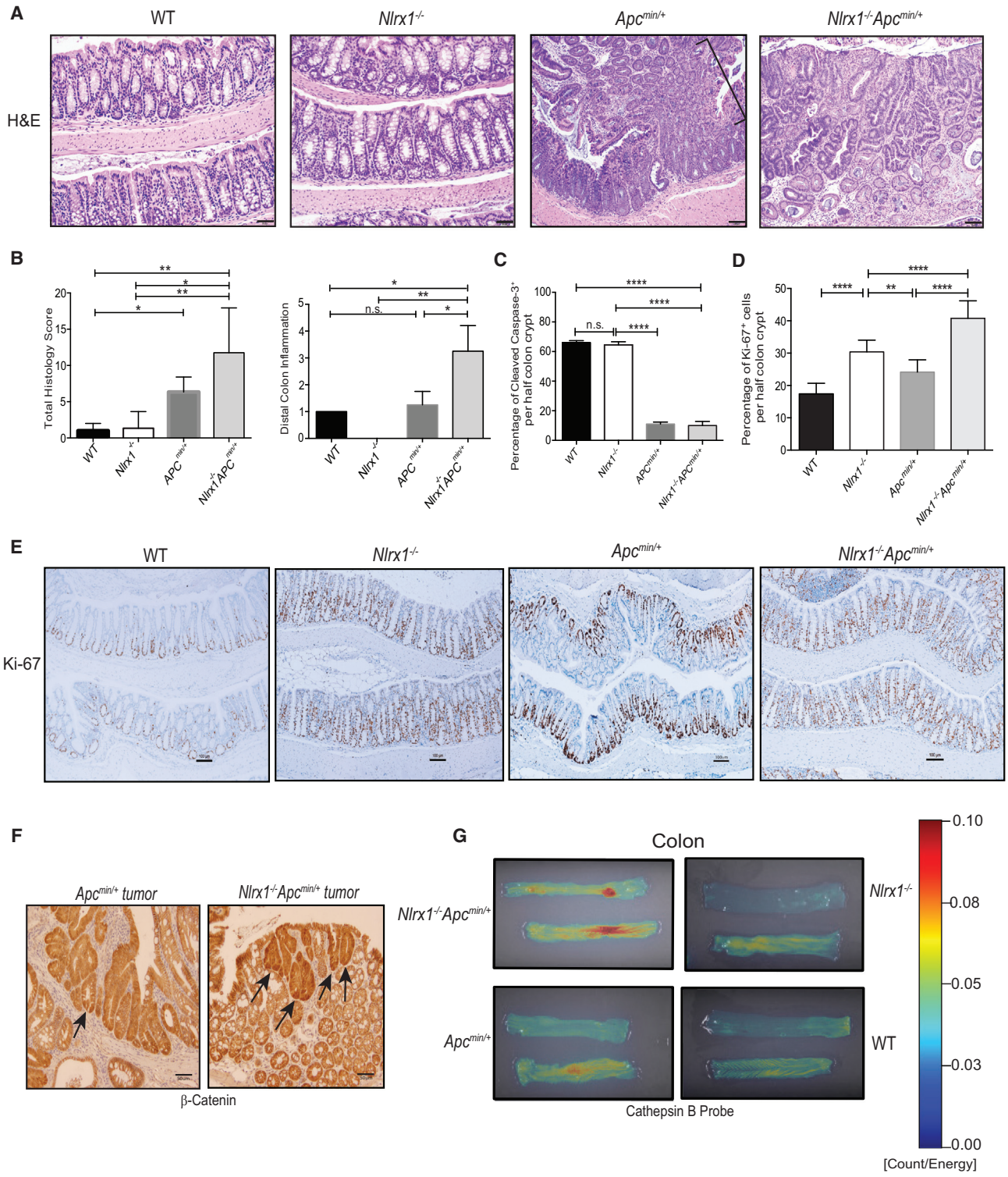

Figure 4. *Nlrx1* Deficiency on the *Apc*$^{min/+}$ Background Leads to Increased Proliferation and Greater Expression of the Tumor Biomarkers β-Catenin and Cathepsin B

(A) Photomicrographs of H&E-stained colons from WT, *Nlrx1*$^{-/-}$, *Apc*$^{min/+}$ mice displayed a pedunculated adenoma (bracket) with mucosal dysplasia, and *Nlrx1*$^{-/-}$*Apc*$^{min/+}$ colons depicted an area of mucosal dysplasia within an adenoma. Scale bars represent 50 μm.

(B) Total Histology score and distal colon inflammation were determined in H&E-stained colon sections represented in A. All slides were scored in a blinded fashion.

(legend continued on next page)

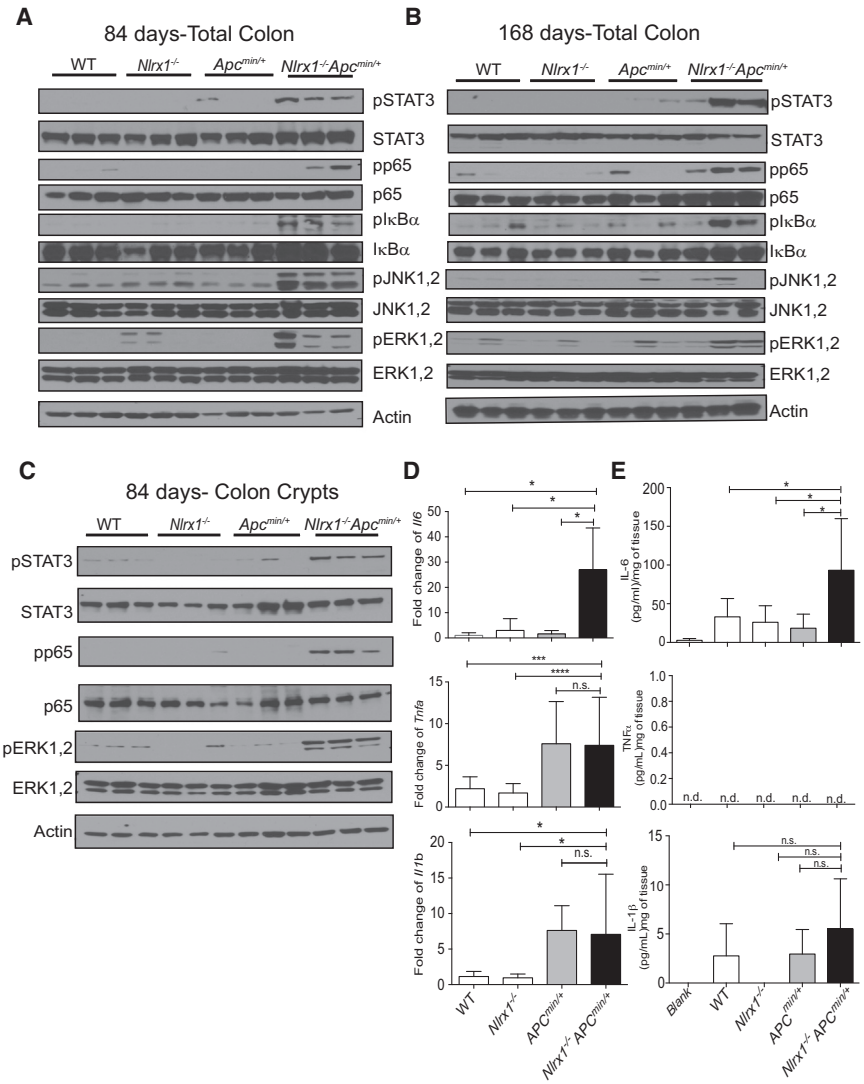

Figure 5. *Nlrx1* Deficiency Contributes to Exacerbated NF-κB, MAPK, and STAT3 Activation and IL-6 Production in the *Apc*$^{min/+}$ Model

(A–C) Protein lysates were isolated from distal colon tissues obtained from WT, *Nlrx1*$^{-/-}$, *Apc*$^{min/+}$, and *Nlrx1*$^{-/-}$*Apc*$^{min/+}$ mice at days 84 (A) and 168 (B), and isolated colon crypts from 84 days (C). Lysates were analyzed by western blot for NF-κB, MAPK, and STAT3 activation. Each lane represents one animal; n ≥ 3 mice/group.

(D) RNA was isolated from age-matched WT, *Nlrx1*$^{-/-}$, *Apc*$^{min/+}$, and *Nlrx1*$^{-/-}$*Apc*$^{min/+}$ distal colonic tissues and analyzed by qPCR for expression levels of *Il6*, *Tnfa*, and *Il1b*, n ≥ 3 mice/group.

(E) IL-6, TNF-α, and IL-1β proteins produced by colon explants were analyzed by ELISA, n ≥ 3 mice/group. n.s., non-significant. *p < 0.05, ***p < 0.001, and ****p < 0.0001.

See also Figure S3.

Oncomine Platform database. This was followed by an examination of newly isolated clinical samples from a Chinese Cohort. Oncomine Platform is an online assembly of microarrays. We analyzed five databases (listed in the Experimental Procedures) that contained information regarding *NLRX1* expression. We first analyzed the Cancer Genome Atlas (TCGA) database, which is the most comprehensive set containing 215 patient and 22 control samples (Cancer Genome Atlas, 2012). This database showed that the expression of *NLRX1* transcript was significantly decreased in colorectal cancer (Figure 7A). Next, we evaluated the expression levels of *NLRX1* transcript at various stages of cancer progression using the TCGA database (Figure 7B). CRC cases were staged according to the staging system determined by the American Joint Committee on Cancer (AJCC) and also known as the tumor-node-metastasis (TNM) system. In stage I, the tumor has spread beyond the inner lining of the colon to the second and third layers of the colon. In stage II, the tumor has spread to the muscle wall of the colon. In stage III, the cancer has metastasized to lymph nodes. In stage IV, the cancer has metastasized to secondary areas of the body such as the liver or lung. This analysis shows that *NLRX1* expression was significantly higher in healthy controls versus all four CRC stages (Figure 7B). Next, we confirmed these findings using four smaller databases within the Oncomine Platform. Significantly lower expression of *NLRX1* was detected in CRC samples in all four databases (Figure 7C). Thus, the composite data from five public databases support the conclusion that *NLRX1* expression is statistically lower in CRC than in healthy colons.

Public database typically do not provide detailed information regarding the patients. Thus, we analyzed mRNA isolated from 40 formalin-fixed and paraffin-embedded (FFPE) CRC samples plus 40 adjacent normal tissues obtained from a Chinese patient

(C–E) Quantification of positive cleaved caspase-3 (C) or Ki-67 (D) cells stained per half-length of crypt was determined from age-matched *Apc*$^{min/+}$ and *Nlrx1*$^{-/-}$*Apc*$^{min/+}$ mice at 168 days of age shown in (E) for Ki-67. n ≥ 4 mice/group, n.s., non-significant. *p < 0.05 **p < 0.01, ***p < 0.001, and ****p < 0.0001. Scale bars represent 100 μm.

(F) Representative histological micrographs of *Apc*$^{min/+}$ and *Nlrx1*$^{-/-}$*Apc*$^{min/+}$ colon tumors at 168 days stained with β-catenin are shown (arrows), n ≥ 3 mice/group. Scale bars represent 50 μm.

(G) Representative images of colons from WT, *Nlrx1*$^{-/-}$, *Apc*$^{min/+}$, and *Nlrx1*$^{-/-}$*Apc*$^{min/+}$ mice at 168 days of age are shown. Fluorescent signals (with intensity scale shown to right) due to active cathepsin B cleavage of target probe were visualized by fluorescence reflectance imaging. n ≥ 2 mice/group.

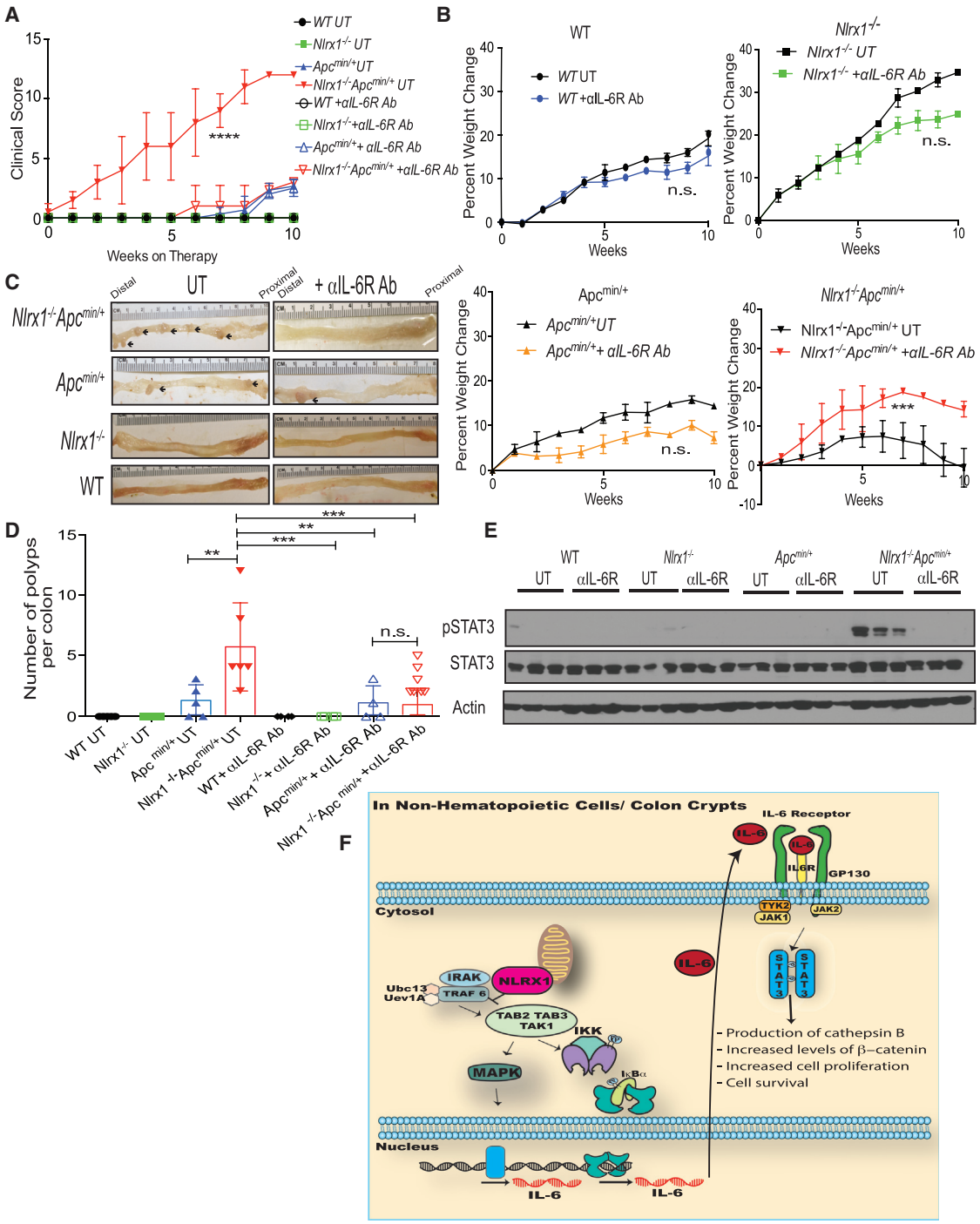

Figure 6. Inhibition of IL-6 Signaling in *Nlrx1*$^{-/-}$*Apc*$^{min/+}$ Mice Reduces Mortality and Tumorigenesis by Decreasing STAT3 Activation

(A) WT, *Nlrx1*$^{-/-}$, *Apc*$^{min/+}$, and *Nlrx1*$^{-/-}$*Apc*$^{min/+}$ animals were subjected to anti-IL6R administration at 20 μg/ml/animal. Cumulative clinical score of animals on and off treatment were monitored.

(B) The percent weight change for animals that were untreated (UT) or given 10 weeks of anti-IL6R therapy is shown for each strain. n ≥ 4 mice/group.

(C) Images are shown of colons isolated at 10 weeks after anti-IL6R therapy from WT, *Nlrx1*$^{-/-}$, *Apc*$^{min/+}$, and *Nlrx1*$^{-/-}$*Apc*$^{min/+}$ animals with polyps indicated (arrows).

(D) Quantification of macroscopic polyp formation in the colons of UT or anti-IL6R-treated animals as indicated. Each data point represents one animal. n ≥ 4 mice/group, n.s., non-significant. *p < 0.05 **p < 0.01, ***p < 0.001, and ****p < 0.0001.

(legend continued on next page)

cohort for the expression of *NLRX1*. The patients selected had not received any chemotherapy or radiotherapy prior to colonic resection. In agreement with Figure 7A, *NLRX1* transcripts were significantly reduced within the CRC samples relative to healthy tissues (Figure 7D). The combined data collected from multiple public databases and an additional cohort of human clinical samples provides overwhelming clinical evidence that *NLRX1* gene expression is reduced in human CRC in comparison to healthy colons, further indicating a critical role for NLRX1 in limiting CRC.

DISCUSSION

The link between cancer and a number of key signaling pathways is well established (Coussens and Werb, 2002). Elevated NF-κB signaling can de-differentiate intestinal epithelial cells that eventually acquire stem-like properties and tumor-initiating capacity (Shaked et al., 2012). NF-κB also facilitates Wnt-driven proliferation of intestinal stem cells, which leads to CRC (Myant et al., 2013; Schwitalla et al., 2013). MAPK regulates intestinal cell proliferation and epithelial differentiation and promotes progression and oncogenesis of human CRC (Dhillon et al., 2007; Lee et al., 2010; Taupin and Podolsky, 1999). NF-κB and STAT3 cooperatively regulate a number of target genes regulating cell cycle and proliferation (Lee et al., 2009; Yang et al., 2007). This work shows that NLRX1 serves as a checkpoint of these multiple critical cancer-promoting pathways to maintain a homeostatic, noncancerous state.

A previous study of NLRX1 in a model that used AOM alone, which is not known to strongly induce tumorigenesis, and a model that involved a short course (3-day) of AOM-DSS treatment, which is unlikely to induce full tumorigenesis, has resulted in conflicting findings regarding the role of NLRX1 (Soares et al., 2014). In contrast, the current study is distinguished by several unique features First, NLRX1 uniformly suppressed colon tumorigenesis in both CAC and sporadic colon cancer models. Second, the loss of *Nlrx1* expression led to heightened IL-6 production and activated STAT3, which are key regulatory pathways in colon cancer that have not been connected to NLR function in tumors. Enhanced NF-κB and ERK activity are known to enhance levels of IL-6, which can lead to STAT3 activation resulting in increased oncogenesis (Corvinus et al., 2005). Cross talk between STAT3 and β-catenin have been documented in different cancers (Armanious et al., 2010; Ibrahem et al., 2014), and STAT3 can also enhance cathepsin B (Dauer et al., 2005), which enhances cancer progression and cell proliferation. Since cathepsin B and β-catenin activity are heightened in $Nlrx1^{-/-}Apc^{min/+}$ mice, inhibitors of these two proteins may be useful in targeting human CRCs with low *NLRX1* expression. Third, while other NLRs such as NLRP3 exert their impact primarily through the hematopoietic compartment, NLRX1 exerts its impact on tumorigenesis mostly via the non-hematopoietic compartment such as colon crypts. Fourth, anti-IL6R therapy effectively decreased tumorigenesis and STAT3 activation in $Nlrx1^{-/-}Apc^{min/+}$ animals. Finally, NLRX1 is also reduced in multiple human CRC patient cohorts, which confers translational relevance to these findings and supports the concept that NLRX1 may serve as a checkpoint against human colon cancer. The discovery of reduced *NLRX1* in human CRC further suggests that *NLRX1* expression may be used as a biomarker of CAC or CRC (Thorsteinsdottir et al., 2011). This finding also has implications for personalized therapy. For example, inhibitors of STAT3 or IL-6, which are Food and Drug Administration (FDA)-approved for other diseases, might be repurposed for controlling human CRCs that have low *NLRX1* expression. Based on the findings in this and previous reports, a working model of how NLRX1 affects tumorigenesis is shown in Figure 6F.

In summary, this report finds that the presence of NLRX1 limits activation of key signaling pathways leading to NF-κB, MAPK, IL-6, and STAT3 activation, which promote various aspects of tumor development. The loss of NLRX1 creates a microenvironment that potentiates the development of tumors in both colitis-associated and sporadic models of CRC. A possible impact is that NLRX1 affects tumor-promoting signals via changes in the microbiome, which would be an important future investigation.

EXPERIMENTAL PROCEDURES

Animals

All studies were conducted in accordance with IACUC guidelines of the University of North Carolina (UNC) at Chapel Hill and NIH guide for the Care and Use of Laboratory Animals. All experiments were performed under SPF conditions using either 6- or 8-week-old male mice or with age as indicated. C57BL/6 (wild-type mice) and $Apc^{min/+}$ mice originated from Jackson Laboratories and were maintained at UNC Chapel Hill for more than nine generations. $Nlrx1^{-/-}$ mice on the C57BL/6 background have been described previously (Moore et al., 2008). $Nlrx1^{-/-}$ mice were crossed with $Apc^{min/+}$ mice to generate $Nlrx1^{-/-}Apc^{min/+}$ mice. Littermates were used as indicated. See the Supplemental Experimental Procedures for colitis and colon cancer models, generation of radiation bone marrow chimeras, and assessment of colon polyps and histopathology.

Assays

Isolation of RNA, tissue extracts, and soluble protein and biochemical and molecular analyses and molecular imaging of proteases are described in the Supplemental Experimental Procedures.

Bioinformatics and Experimental Analysis of *NLRX1* Expression in Human CRC

Microarray studies from the Oncomine Platform containing data describing *NLRX1* expression in CRC and the collection and processing of human CRC specimens are described in the Supplemental Experimental Procedures.

Statistics

All results are presented as the mean ± SEM. Significance between two groups was assessed by the Student's two-tailed t test. Datasets that had more than two sets of data for analysis were analyzed by ANOVA with Tukey–Kramer HSD post test for multiple comparisons to determine significance. The product limit method of Kaplan-Meier was utilized for generating the survival curves, which were compared using the log rank test. See the

(E) Protein lysates were isolated from distal colon tissues obtained from WT, $Nlrx1^{-/-}$, $Apc^{min/+}$, and $Nlrx1^{-/-}Apc^{min/+}$ mice that were either left UT or were treated with anti-IL6R for 10 weeks. Lysates were analyzed by western blot for phosphorylated STAT3. Each band represents one animal; $n \geq 3$ mice/group.
(F) Model of NLRX1 negatively impacting NF-κB and MAPK, which increase IL-6 to activate STAT3 and the downstream oncogenic cathepsin B and β-catenin pathways to increase proliferation in tumors.

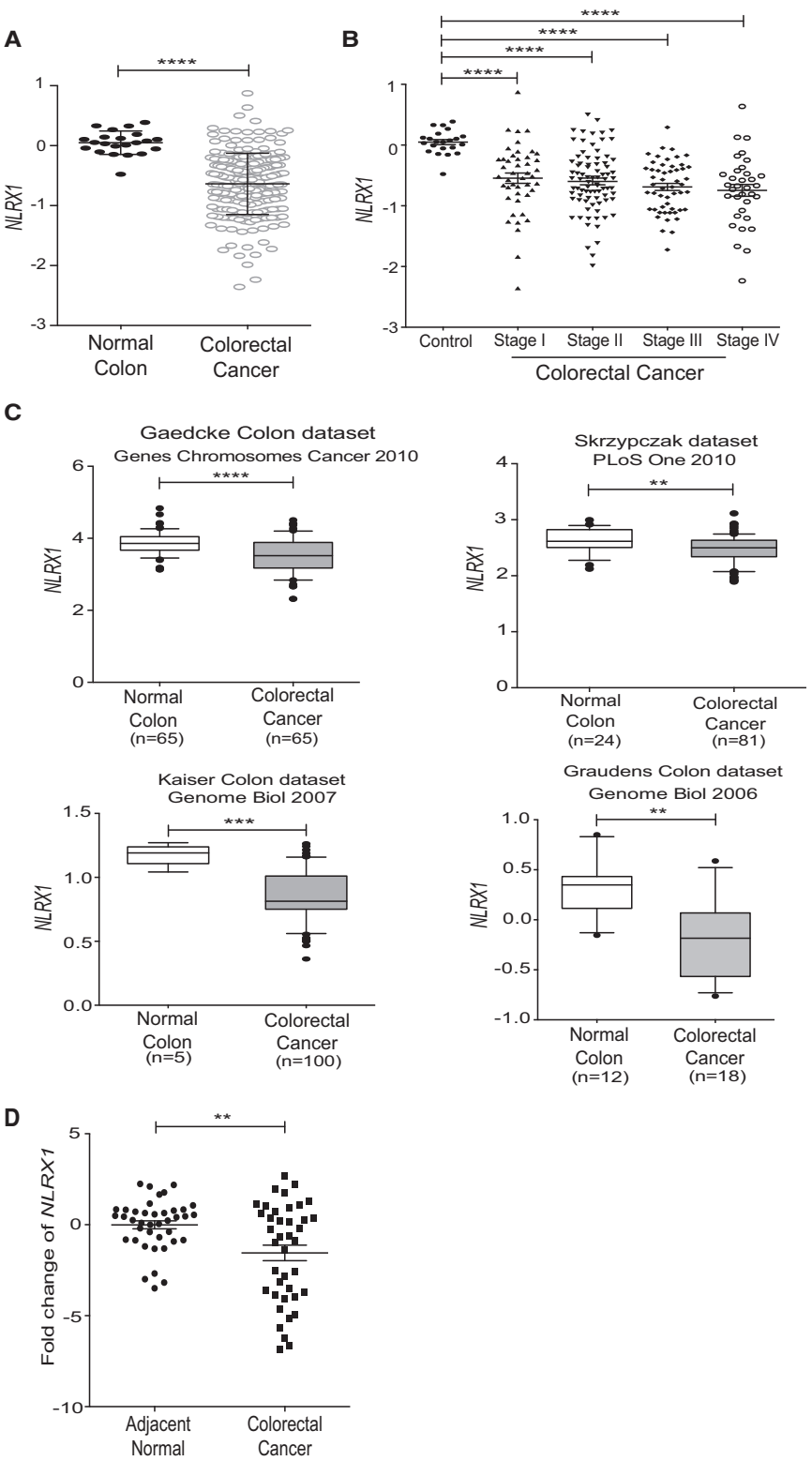

Figure 7. *NLRX1* Expression Is Reduced in Multiple Colorectal Cancer Patient Databases and in Clinical Samples

(A) CRC microarray databases were mined for *NLRX1* expression. The raw data were exported from the TCGA CRC database, with representations of 22 healthy control and 215 CRC samples. Mean ± SEM, presented as Log2 median-centered ratio expression. Unpaired Mann-Whitney test was used to evaluate the statistical significance.

(B) Correlation analysis compared expression levels of *NLRX1* among different stages of CRC progression. TNM stage information was exported from the TCGA colon database.

(C) Reduced *NLRX1* expression was found in four additional CRC databases. Log2 median-centered ratio expression is presented for the four datasets used. Box plots were generated by GraphPad, whiskers are drawn down to the 10th percentile and up to the 90th percentile. Points below and above the whiskers are drawn as individual dots.

(D) *NLRX1* expression in human clinical CRC FFPE samples collected from a Chinese patient cohort (n = 40) was analyzed by qPCR using comparative C_T method ($2^{-\Delta\Delta CT}$) (mean ± SEM). **p < 0.01, ***p < 0.001, and ****p < 0.0001.

Supplemental Experimental Procedures for statistics used with clinical human samples.

SUPPLEMENTAL INFORMATION

Supplemental Information includes Supplemental Experimental Procedures and three figures and can be found with this article online at http://dx.doi.org/10.1016/j.celrep.2016.02.064.

AUTHOR CONTRIBUTIONS

A.A.K., A.D.T., and J.P.-Y.T. designed experiments and wrote manuscript with insight from J.E.W., W.J.B., S.D., and P.K.L. A.A.K. performed immunoblots and analyses. A.D.T. and R.L. performed qPCR and analyses. A.A.K., A.D.T., W.J.B., J.E.W., and S.D. conducted CAC and *Apc*$^{min/+}$ mouse studies. R.L. and A.D.T. prepared human samples and analyzed datasets. S.D. performed FRI of intestinal tissues. P.H. and Z.L. obtained human samples. M.M., R.T.M., and C.J. performed mini-endoscopy. S.A.M. analyzed H&E slides and provided histopathological scoring. All contributing authors have agreed to submission of manuscript for publication.

ACKNOWLEDGMENTS

This project was supported in part by NIH grants CA156330 (to J.P.-Y.T. and A.A.K.), AI029564, DK094779, 5-T32-LCCC (to LCCC), T32-DK007737 (to UNC Gastroenterology Research Training), DK047769 (to S.D. and P.K.L.), and F32-DK098916 (to A.D.T.). J.E.W. was supported by the American Cancer Society (PF-13-401-01-TBE). Animal histopathology was performed within the LCCC Animal Histopathology Core Facility at UNC, supported in part by the National Cancer Institute (CA16086).

Received: July 29, 2015
Revised: February 8, 2016
Accepted: February 19, 2016
Published: March 10, 2016

REFERENCES

Abdul-Sater, A.A., Saïd-Sadier, N., Lam, V.M., Singh, B., Pettengill, M.A., Soares, F., Tattoli, I., Lipinski, S., Girardin, S.E., Rosenstiel, P., and Ojcius, D.M. (2010). Enhancement of reactive oxygen species production and chlamydial infection by the mitochondrial Nod-like family member NLRX1. J. Biol. Chem. *285*, 41637–41645.

Allen, I.C., TeKippe, E.M., Woodford, R.M., Uronis, J.M., Holl, E.K., Rogers, A.B., Herfarth, H.H., Jobin, C., and Ting, J.P. (2010). The NLRP3 inflammasome functions as a negative regulator of tumorigenesis during colitis-associated cancer. J. Exp. Med. *207*, 1045–1056.

Allen, I.C., Moore, C.B., Schneider, M., Lei, Y., Davis, B.K., Scull, M.A., Gris, D., Roney, K.E., Zimmermann, A.G., Bowzard, J.B., et al. (2011). NLRX1 protein attenuates inflammatory responses to infection by interfering with the RIG-I-MAVS and TRAF6-NF-κB signaling pathways. Immunity *34*, 854–865.

Allen, I.C., Wilson, J.E., Schneider, M., Lich, J.D., Roberts, R.A., Arthur, J.C., Woodford, R.M., Davis, B.K., Uronis, J.M., Herfarth, H.H., et al. (2012). NLRP12 suppresses colon inflammation and tumorigenesis through the negative regulation of noncanonical NF-κB signaling. Immunity *36*, 742–754.

Allocca, M., Jovani, M., Fiorino, G., Schreiber, S., and Danese, S. (2013). Anti-IL-6 treatment for inflammatory bowel diseases: next cytokine, next target. Curr. Drug Targets *14*, 1508–1521.

Anand, P.K., Malireddi, R.K., Lukens, J.R., Vogel, P., Bertin, J., Lamkanfi, M., and Kanneganti, T.D. (2012). NLRP6 negatively regulates innate immunity and host defence against bacterial pathogens. Nature *488*, 389–393.

Armanious, H., Gelebart, P., Mackey, J., Ma, Y., and Lai, R. (2010). STAT3 upregulates the protein expression and transcriptional activity of β-catenin in breast cancer. Int. J. Clin. Exp. Pathol. *3*, 654–664.

Atreya, R., and Neurath, M.F. (2005). Involvement of IL-6 in the pathogenesis of inflammatory bowel disease and colon cancer. Clin. Rev. Allergy Immunol. *28*, 187–196.

Bailey, C.E., Hu, C.Y., You, Y.N., Bednarski, B.K., Rodriguez-Bigas, M.A., Skibber, J.M., Cantor, S.B., and Chang, G.J. (2015). Increasing disparities in the age-related incidences of colon and rectal cancers in the United States, 1975-2010. JAMA Surg. *150*, 17–22.

Becker, C., Fantini, M.C., Wirtz, S., Nikolaev, A., Lehr, H.A., Galle, P.R., Rose-John, S., and Neurath, M.F. (2005). IL-6 signaling promotes tumor growth in colorectal cancer. Cell Cycle *4*, 217–220.

Ben-Neriah, Y., and Karin, M. (2011). Inflammation meets cancer, with NF-κB as the matchmaker. Nat. Immunol. *12*, 715–723.

Bollrath, J., Phesse, T.J., von Burstin, V.A., Putoczki, T., Bennecke, M., Bateman, T., Nebelsiek, T., Lundgren-May, T., Canli, O., Schwitalla, S., et al. (2009). gp130-mediated Stat3 activation in enterocytes regulates cell survival and cell-cycle progression during colitis-associated tumorigenesis. Cancer Cell *15*, 91–102.

Cancer Genome Atlas, N.; Cancer Genome Atlas Network (2012). Comprehensive molecular characterization of human colon and rectal cancer. Nature *487*, 330–337.

Chen, G.Y., Liu, M., Wang, F., Bertin, J., and Núñez, G. (2011). A functional role for Nlrp6 in intestinal inflammation and tumorigenesis. J. Immunol. *186*, 7187–7194.

Clevers, H., and Nusse, R. (2012). Wnt/β-catenin signaling and disease. Cell *149*, 1192–1205.

Corvinus, F.M., Orth, C., Moriggl, R., Tsareva, S.A., Wagner, S., Pfitzner, E.B., Baus, D., Kaufmann, R., Huber, L.A., Zatloukal, K., et al. (2005). Persistent STAT3 activation in colon cancer is associated with enhanced cell proliferation and tumor growth. Neoplasia *7*, 545–555.

Coussens, L.M., and Werb, Z. (2002). Inflammation and cancer. Nature *420*, 860–867.

Dauer, D.J., Ferraro, B., Song, L., Yu, B., Mora, L., Buettner, R., Enkemann, S., Jove, R., and Haura, E.B. (2005). Stat3 regulates genes common to both wound healing and cancer. Oncogene *24*, 3397–3408.

Dhillon, A.S., Hagan, S., Rath, O., and Kolch, W. (2007). MAP kinase signalling pathways in cancer. Oncogene *26*, 3279–3290.

Ding, S., Blue, R.E., Morgan, D.R., and Lund, P.K. (2014). Comparison of multiple enzyme activatable near-infrared fluorescent molecular probes for detection and quantification of inflammation in murine colitis models. Inflamm. Bowel Dis. *20*, 363–377.

Ditsworth, D., and Zong, W.X. (2004). NF-kappaB: key mediator of inflammation-associated cancer. Cancer Biol. Ther. *3*, 1214–1216.

Dupaul-Chicoine, J., Yeretssian, G., Doiron, K., Bergstrom, K.S., McIntire, C.R., LeBlanc, P.M., Meunier, C., Turbide, C., Gros, P., Beauchemin, N., et al. (2010). Control of intestinal homeostasis, colitis, and colitis-associated colorectal cancer by the inflammatory caspases. Immunity *32*, 367–378.

Elinav, E., Strowig, T., Kau, A.L., Henao-Mejia, J., Thaiss, C.A., Booth, C.J., Peaper, D.R., Bertin, J., Eisenbarth, S.C., Gordon, J.I., and Flavell, R.A. (2011). NLRP6 inflammasome regulates colonic microbial ecology and risk for colitis. Cell *145*, 745–757.

Elinav, E., Nowarski, R., Thaiss, C.A., Hu, B., Jin, C., and Flavell, R.A. (2013). Inflammation-induced cancer: crosstalk between tumours, immune cells and microorganisms. Nat. Rev. Cancer *13*, 759–771.

Fleming, M., Ravula, S., Tatishchev, S.F., and Wang, H.L. (2012). Colorectal carcinoma: Pathologic aspects. J. Gastrointest. Oncol. *3*, 153–173.

Fodde, R., Smits, R., and Clevers, H. (2001). APC, signal transduction and genetic instability in colorectal cancer. Nat. Rev. Cancer *1*, 55–67.

Gounaris, E., Martin, J., Ishihara, Y., Khan, M.W., Lee, G., Sinh, P., Chen, E.Z., Angarone, M., Weissleder, R., Khazaie, K., and Barrett, T.A. (2013). Fluorescence endoscopy of cathepsin activity discriminates dysplasia from colitis. Inflamm. Bowel Dis. *19*, 1339–1345.

Please cite this article in press as: Koblansky et al., The Innate Immune Receptor NLRX1 Functions as a Tumor Suppressor by Reducing Colon Tumorigenesis and Key Tumor-Promoting Signals, Cell Reports (2016), http://dx.doi.org/10.1016/j.celrep.2016.02.064

Greten, F.R., Eckmann, L., Greten, T.F., Park, J.M., Li, Z.W., Egan, L.J., Kagnoff, M.F., and Karin, M. (2004). IKKbeta links inflammation and tumorigenesis in a mouse model of colitis-associated cancer. Cell *118*, 285–296.

Grivennikov, S., Karin, E., Terzic, J., Mucida, D., Yu, G.Y., Vallabhapurapu, S., Scheller, J., Rose-John, S., Cheroutre, H., Eckmann, L., and Karin, M. (2009). IL-6 and Stat3 are required for survival of intestinal epithelial cells and development of colitis-associated cancer. Cancer Cell *15*, 103–113.

Hayden, M.S., and Ghosh, S. (2011). NF-κB in immunobiology. Cell Res. *21*, 223–244.

Heyer, J., Yang, K., Lipkin, M., Edelmann, W., and Kucherlapati, R. (1999). Mouse models for colorectal cancer. Oncogene *18*, 5325–5333.

Hugot, J.-P., Chamaillard, M., Zouali, H., Lesage, S., Cézard, J.-P., Belaiche, J., Almer, S., Tysk, C., O'Morain, C.A., Gassull, M., et al. (2001). Association of NOD2 leucine-rich repeat variants with susceptibility to Crohn's disease. Nature *411*, 599–603.

Hyams, J.S., Fitzgerald, J.E., Treem, W.R., Wyzga, N., and Kreutzer, D.L. (1993). Relationship of functional and antigenic interleukin 6 to disease activity in inflammatory bowel disease. Gastroenterology *104*, 1285–1292.

Ibrahem, S., Al-Ghamdi, S., Baloch, K., Muhammad, B., Fadhil, W., Jackson, D., Nateri, A.S., and Ilyas, M. (2014). STAT3 paradoxically stimulates β-catenin expression but inhibits β-catenin function. Int. J. Exp. Pathol. *95*, 392–400.

Kang, M.J., Yoon, C.M., Kim, B.H., Lee, C.M., Zhou, Y., Sauler, M., Homer, R., Dhamija, A., Boffa, D., West, A.P., et al. (2015). Suppression of NLRX1 in chronic obstructive pulmonary disease. J. Clin. Invest. *125*, 2458–2462.

Kinzler, K.W., and Vogelstein, B. (1996). Lessons from hereditary colorectal cancer. Cell *87*, 159–170.

Kuester, D., Lippert, H., Roessner, A., and Krueger, S. (2008). The cathepsin family and their role in colorectal cancer. Pathol. Res. Pract. *204*, 491–500.

Kurzawski, G., Suchy, J., Kładny, J., Grabowska, E., Mierzejewski, M., Jakubowska, A., Debniak, T., Cybulski, C., Kowalska, E., Szych, Z., et al. (2004). The NOD2 3020insC mutation and the risk of colorectal cancer. Cancer Res. *64*, 1604–1606.

Lee, H., Herrmann, A., Deng, J.-H., Kujawski, M., Niu, G., Li, Z., Forman, S., Jove, R., Pardoll, D.M., and Yu, H. (2009). Persistently activated Stat3 maintains constitutive NF-kappaB activity in tumors. Cancer Cell *15*, 283–293.

Lee, S.H., Hu, L.L., Gonzalez-Navajas, J., Seo, G.S., Shen, C., Brick, J., Herdman, S., Varki, N., Corr, M., Lee, J., and Raz, E. (2010). ERK activation drives intestinal tumorigenesis in Apc(min/+) mice. Nat. Med. *16*, 665–670.

Lin, W.W., and Karin, M. (2007). A cytokine-mediated link between innate immunity, inflammation, and cancer. J. Clin. Invest. *117*, 1175–1183.

Moore, C.B., Bergstralh, D.T., Duncan, J.A., Lei, Y., Morrison, T.E., Zimmermann, A.G., Accavitti-Loper, M.A., Madden, V.J., Sun, L., Ye, Z., et al. (2008). NLRX1 is a regulator of mitochondrial antiviral immunity. Nature *451*, 573–577.

Myant, K.B., Cammareri, P., McGhee, E.J., Ridgway, R.A., Huels, D.J., Cordero, J.B., Schwitalla, S., Kalna, G., Ogg, E.L., Athineos, D., et al. (2013). ROS production and NF-κB activation triggered by RAC1 facilitate WNT-driven intestinal stem cell proliferation and colorectal cancer initiation. Cell Stem Cell *12*, 761–773.

Neufert, C., Becker, C., and Neurath, M.F. (2007). An inducible mouse model of colon carcinogenesis for the analysis of sporadic and inflammation-driven tumor progression. Nat. Protoc. *2*, 1998–2004.

O'Shea, J.J., Holland, S.M., and Staudt, L.M. (2013). JAKs and STATs in immunity, immunodeficiency, and cancer. N. Engl. J. Med. *368*, 161–170.

Ogura, Y., Bonen, D.K., Inohara, N., Nicolae, D.L., Chen, F.F., Ramos, R., Britton, H., Moran, T., Karaliuskas, R., Duerr, R.H., et al. (2001). A frameshift mutation in NOD2 associated with susceptibility to Crohn's disease. Nature *411*, 603–606.

Rogler, G. (2014). Chronic ulcerative colitis and colorectal cancer. Cancer Lett. *345*, 235–241.

Schwitalla, S., Fingerle, A.A., Cammareri, P., Nebelsiek, T., Göktuna, S.I., Ziegler, P.K., Canli, O., Heijmans, J., Huels, D.J., Moreaux, G., et al. (2013). Intestinal tumorigenesis initiated by dedifferentiation and acquisition of stem-cell-like properties. Cell *152*, 25–38.

Sebolt-Leopold, J.S., and Herrera, R. (2004). Targeting the mitogen-activated protein kinase cascade to treat cancer. Nat. Rev. Cancer *4*, 937–947.

Shaked, H., Hofseth, L.J., Chumanevich, A., Chumanevich, A.A., Wang, J., Wang, Y., Taniguchi, K., Guma, M., Shenouda, S., Clevers, H., et al. (2012). Chronic epithelial NF-κB activation accelerates APC loss and intestinal tumor initiation through iNOS up-regulation. Proc. Natl. Acad. Sci. USA *109*, 14007–14012.

Siegel, R., Naishadham, D., and Jemal, A. (2013). Cancer statistics, 2013. CA Cancer J. Clin. *63*, 11–30.

Soares, F., Tattoli, I., Rahman, M.A., Robertson, S.J., Belcheva, A., Liu, D., Streutker, C., Winer, S., Winer, D.A., Martin, A., et al. (2014). The mitochondrial protein NLRX1 controls the balance between extrinsic and intrinsic apoptosis. J. Biol. Chem. *289*, 19317–19330.

Staudt, L.M. (2010). Oncogenic activation of NF-kappaB. Cold Spring Harb. Perspect. Biol. *2*, a000109.

Takeuchi, O., and Akira, S. (2010). Pattern recognition receptors and inflammation. Cell *140*, 805–820.

Tattoli, I., Carneiro, L.A., Jéhanno, M., Magalhaes, J.G., Shu, Y., Philpott, D.J., Arnoult, D., and Girardin, S.E. (2008). NLRX1 is a mitochondrial NOD-like receptor that amplifies NF-kappaB and JNK pathways by inducing reactive oxygen species production. EMBO Rep. *9*, 293–300.

Taupin, D., and Podolsky, D.K. (1999). Mitogen-activated protein kinase activation regulates intestinal epithelial differentiation. Gastroenterology *116*, 1072–1080.

Terzić, J., Grivennikov, S., Karin, E., and Karin, M. (2010). Inflammation and colon cancer. Gastroenterology *138*, 2101–2114.e5.

Thorsteinsdottir, S., Gudjonsson, T., Nielsen, O.H., Vainer, B., and Seidelin, J.B. (2011). Pathogenesis and biomarkers of carcinogenesis in ulcerative colitis. Nat. Rev. Gastroenterol. Hepatol. *8*, 395–404.

Waldner, M.J., Foersch, S., and Neurath, M.F. (2012). Interleukin-6–a key regulator of colorectal cancer development. Int. J. Biol. Sci. *8*, 1248–1253.

Wullaert, A., Bonnet, M.C., and Pasparakis, M. (2011). NF-κB in the regulation of epithelial homeostasis and inflammation. Cell Res. *21*, 146–158.

Xia, X., Cui, J., Wang, H.Y., Zhu, L., Matsueda, S., Wang, Q., Yang, X., Hong, J., Songyang, Z., Chen, Z.J., and Wang, R.F. (2011). NLRX1 negatively regulates TLR-induced NF-κB signaling by targeting TRAF6 and IKK. Immunity *34*, 843–853.

Yang, J., Liao, X., Agarwal, M.K., Barnes, L., Auron, P.E., and Stark, G.R. (2007). Unphosphorylated STAT3 accumulates in response to IL-6 and activates transcription by binding to NFkappaB. Genes Dev. *21*, 1396–1408.

Yashiro, M. (2014). Ulcerative colitis-associated colorectal cancer. World J. Gastroenterol. *20*, 16389–16397.

Zaki, M.H., Boyd, K.L., Vogel, P., Kastan, M.B., Lamkanfi, M., and Kanneganti, T.D. (2010). The NLRP3 inflammasome protects against loss of epithelial integrity and mortality during experimental colitis. Immunity *32*, 379–391.

Zaki, M.H., Vogel, P., Malireddi, R.K., Body-Malapel, M., Anand, P.K., Bertin, J., Green, D.R., Lamkanfi, M., and Kanneganti, T.D. (2011). The NOD-like receptor NLRP12 attenuates colon inflammation and tumorigenesis. Cancer Cell *20*, 649–660.

Cell Reports, Volume *14*

Supplemental Information

The Innate Immune Receptor NLRX1 Functions as a Tumor Suppressor by Reducing Colon Tumorigenesis and Key Tumor-Promoting Signals

A. Alicia Koblansky, Agnieszka D. Truax, Rongrong Liu, Stephanie A. Montgomery, Shengli Ding, Justin E. Wilson, W. June Brickey, Marcus Mühlbauer, Rita-Marie T. McFadden, Peizhen Hu, Zengshan Li, Christian Jobin, Pauline Kay Lund, and Jenny P.-Y. Ting

Supplemental Figures

A

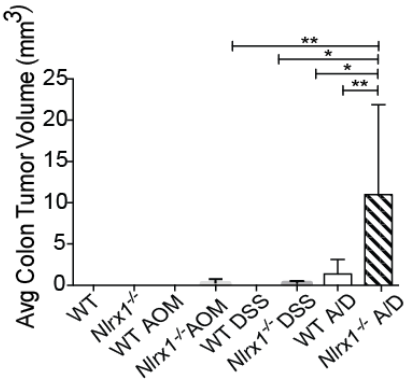

B

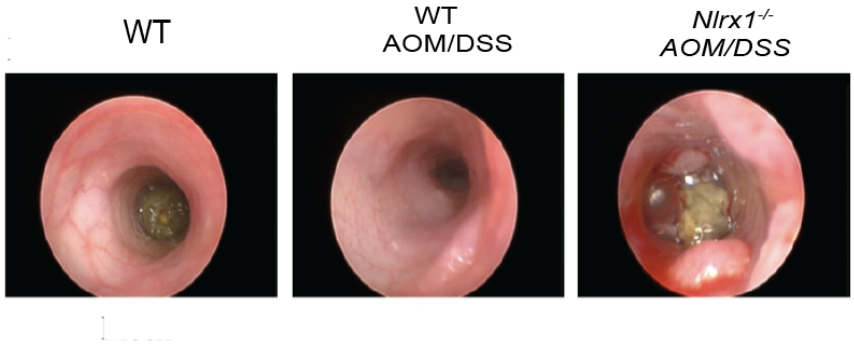

Figure S1

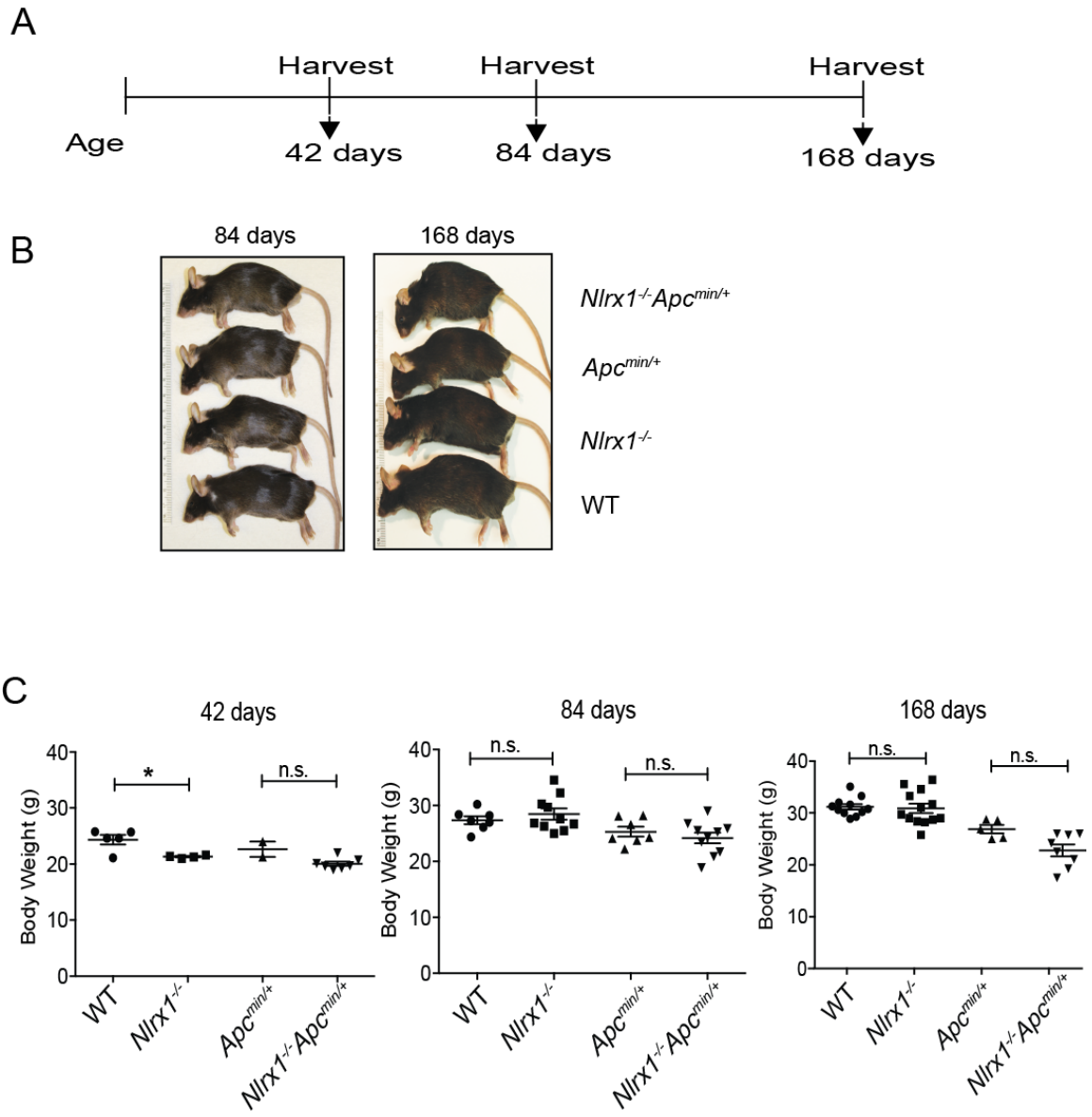
A
Harvest
Harvest
Harvest
Age
42 days
84 days
168 days
B
84 days
168 days
Nlrx1-/-Apcmin/+
Apcmin/+
Nlrx1-/-
WT
C
42 days
84 days
168 days
Body Weight (g)
0
10
20
30
40
*
n.s.
WT
Nlrx1-/-
Apcmin/+
Nlrx1-/-Apcmin/+

Figure S2

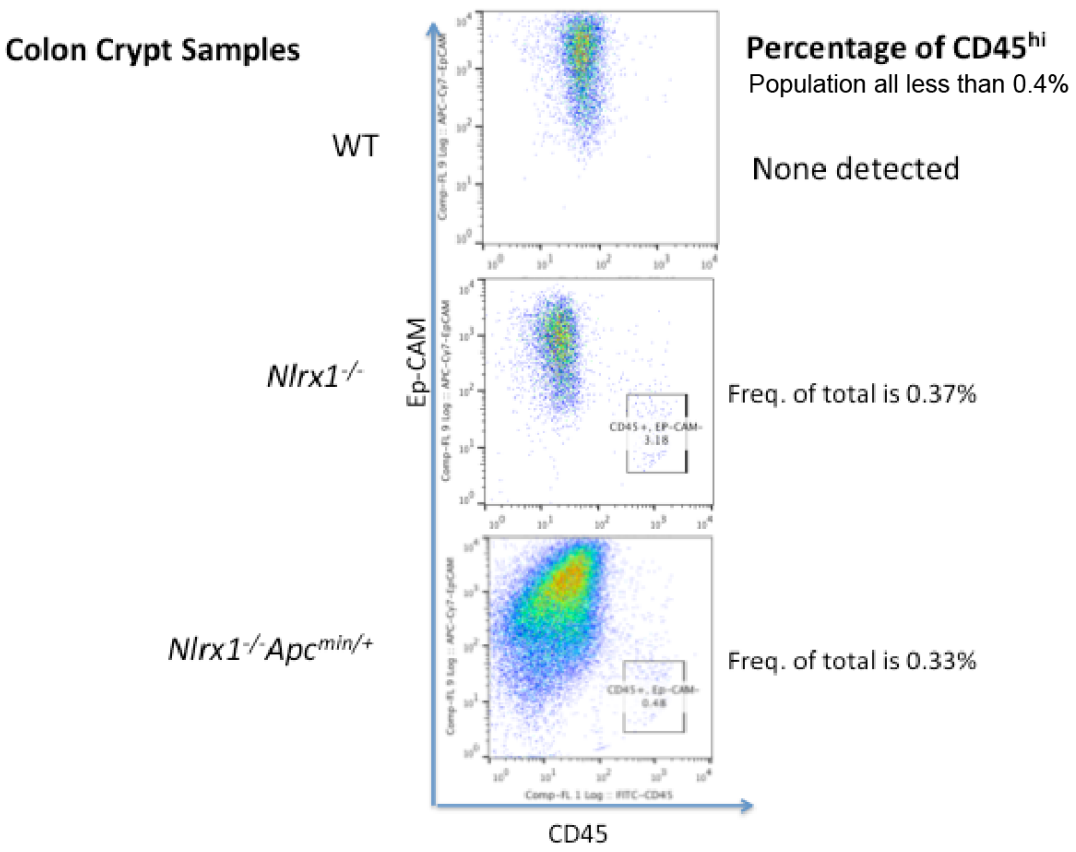
Colon Crypt Samples
Percentage of CD45hi
Population all less than 0.4%
WT
None detected
Nlrx1-/-
Freq. of total is 0.37%
Nlrx1-/-Apcmin/+
Freq. of total is 0.33%
Ep-CAM
CD45
CD45+, EP-CAM- 3.18
CD45+, Ep-CAM- 0.48

Figure S3

SUPPLEMENTAL FIGURE LEGENDS

Figure S1 (related to Figure 1): After AOM/DSS treatment, *Nlrx1*$^{-/-}$ mice have increased tumor burden compared to WT animals. (A) *Nlrx1*$^{-/-}$ animals have significantly increased tumor volume compared to WT animals during AOM/DSS-induced CAC. Tumor volumes were determined as the average sum of the volumes [V = (width^2 x length)/2] of all colon tumors per mouse**.** (B) *Nlrx1*$^{-/-}$ and WT mice challenged with AOM and 3% DSS showed more polyps as assessed by an endoscopic examination. Endoscopy of untreated WT mice and AOM/DSS-treated WT and *Nlrx1*$^{-/-}$ mice forty-eight days after the first DSS treatment. Images are representative of two mice for each condition.

Figure S2 (related to Figure 3): *Nlrx1*$^{-/-}$*Apc*$^{min/+}$ mice display a more severe phenotype, but no significant difference in weight compared to controls. (A) Schematic of harvest times of indicated animals at 168, 84, and 42 days of age to elucidate potential causes of early mortality in the *Apc*$^{min/+}$ model. (B) Images of WT*, Nlrx1*$^{-/-}$*, Apc*$^{min/+}$ and *Nlrx1*$^{-/-}$*Apc*$^{min/+}$ mice at 84 and 168 days of age. (C) Comparison of body weights from *Nlrx1*$^{-/-}$*Apc*$^{Min/+}$, *APC*$^{min/+}$, *Nlrx1*$^{-/-}$ and WT mice at 42, 84 and 168 days. Each data point represents one animal. n.s., non-significant, *p<0.05, **p<0.01 and ****p<0.0001.

Figure S3 (Related to Figure 5): FACS analysis of colon crypts. Colon crypt cells were collected from four different strains of mice: WT, *Nlrx1*$^{-/-}$, *APC*$^{min/+,}$ and

Nlrx1$^{-/-}$*Apc*$^{min/+}$. Cells were stained with both CD45-FITC and EpCAM-APC in FACS staining buffer. FACS analysis revealed that the isolated colon crypt cells were EpCAM^{Hi} and CD45^{Lo}. The frequency of CD45^{+} cells in the colon crypt cell populations were determine to be < 0.4%.

SUPPLEMENTAL EXPERIMENTAL PROCEDURES:

Animals: All experiments were performed under specific-pathogen-free (SPF) conditions. Sentinel mice were routinely monitored for bacterial, viral, ecto, and endoparasitic pathogens so to confirm SPF condition. For littermates, heterozygous mice were breed and maintained for experimental work.

Induction of experimental chronic colitis and colitis-associated colon cancer (CAC): To induce chronic colitis, littermates were given three cycles of 3% DSS for 5 days followed by 14 days of regular drinking water (Neufert et al., 2007). To Induce CAC, animals were given a single i.p. injection of the mutagen azoxymethane (AOM, 10 mg/kg body weight) (Sigma-Aldrich) in combination with three cycles of 3% DSS in drinking water for 5 days followed by regular drinking water for 14 days. Animals were euthanized at the end of the study on day 55 or when moribund with weight loss greater than 20% as stated in our IACUC-approved protocol. Animals were monitored for weight loss daily during DSS treatment and once every two days during regular water administration to measure disease progression. Furthermore, clinical score assessments were blindly performed after each round of DSS at days 7, 26, and 45, which consisted assessments of body condition, stool consistency, rectal bleeding and presence of stool blood measured using Hemoccult Immunochemical Fecal Occult (Beckman Coulter) as previously described (Allen et al., 2010). Tumor volumes were determined as the average sum of the volumes [$V = (\text{width}^2 \times \text{length})/2$] of all colon tumors per mouse.

Radiation bone marrow chimeras: Radiation bone marrow chimeric mice were generated as previously described (Allen et al., 2010). Briefly, 10-12 week-old wild type ($CD45.1^+$) and *Nlrx1*$^{-/-}$ (CD45.2) mice were lethally irradiated (10 Gy) and i.v. injected with 10^7 bone marrow cells isolated from either wild type $CD45.1^+$ or *Nlrx1*$^{-/-}$ mice 24 hours post total body irradiation. Recipient mice were given 2 mg/ml neomycin in drinking water for 14 days and housed for an additional 56 days to allow for full bone marrow reconstitution before administration of AOM/DSS.

Molecular imaging of proteases: To quantify cathepsin B activity, an indirect imaging approach using a cathepsin B-catalyzable fluorescent target as described previously (Ding et al., 2014; Ding et al., 2012) was utilized. Specifically, the Near Infrared Fluorescence imaging probe ProSense 680 (PerkinElmer, Cat# NEV10003) emits a signal when activated by proteases with the highest specificity demonstrated by cathepsin B (Jaffer et al., 2008) and has been used for intestinal tumor detection (Zhang et al., 2008). The probe was administered to mice via retro-orbital injection. Animals were euthanized by an i.p. injection of Nembutal (100 mg/kg body weight) 24 hours later, and gastrointestinal tissues were harvested. Each part of colon was gently flushed with ice cold 1X PBS and imaged *ex vivo* by fluorescence reflectance imaging (FRI) (FMT 2500™ LX System, PerkinElmer). The light source energy level, exposure time and the distance from specimen to camera were kept constant across animals. During FRI imaging, the imaging system automatically adjusts

the scale to encompass the minimum-maximum of the signal for optimal visualization, with a higher scale reflecting a stronger signal.

Assessment of colon polyps: *In situ* mini-endoscopy was used to visualize *in vivo* tumor formation in mouse colons. Prior to endoscopy, animals were fasted overnight to minimize fecal obstruction. Endoscopy was performed by a trained gastroenterologist (M.M.) on animals under oxygen-regulated isoflurane (Minrad, Inc) sedation on day 48 of the AOM/DSS model using a Coloview system (Karl Storz Veterinary Endoscope) as previously described (Uronis et al., 2009). Colons were air inflated for real time visualization of 3-4 cm of colon from anal verge to the splenic flexure. The gastroenterologist was blinded to the genotype and experimental conditions. In addition, upon the completion of the AOM/DSS model, animals were euthanized and colons were removed, flushed with PBS and open longitudinally for visual polyp count.

Histopathology and immunohistochemistry: To visualize tissue pathology, isolated colons were flushed with PBS, prepared as Swiss rolls, fixed in 10% formalin and embedded in paraffin. Hematoxylin and eosin (H&E) staining was performed on 5-micron-thick sections, and hyperplasia and dysplasia were blindly evaluated by a Board-certified veterinary pathologist. Briefly, individual lesions were scored as described previously (Meira et al., 2008), and a total histology score for each specimen was completed by summing the individual lesion scores. Additional sections were stained for the tumorigenesis marker β-

catenin [E247] (Abcam), cleaved Caspase-3 (Abcam), and and Ki67 (Vector Laboratories). Measurements for percentage of cleaved Caspase-3^+ and Ki-67^+ cells were collected from 20 crypts that were sectioned longitudinal; half length of each colon crypt was measured from the basal layer. This was performed on three independent mice per strain.

RNA isolation and analysis: Inflammatory cytokine expression during colitis and CAC was assessed by washing colons with PBS and homogenizing the distal-most section for total RNA extraction using Trizol (Invitrogen). Following RNA isolation, total RNA was eluted with distilled water, and the RNA concentration was measured using a Nanodrop 2000 spectrophotometer. Subsequently iScript™ cDNA Synthesis Kit 170-8891 (Bio-Rad Laboratories, Inc.) was used to generate cDNA. Quantitative RT-PCR was performed on a ViiA™ 7 Real-Time PCR System. Quantitative PCR for mouse *Il1b* (Mm00434228_m1)*, Il6* (Mm00446190_m1) and *Tnfa* (Mm00443258_m1) was performed using TaqMan primer/probe sets and master mix (Applied Biosystems). To normalize the qPCR results, *Gapdh* (Mm99999915_g1) and *Actb* (Mm01324804_m1) were chosen as reference genes. All samples were loaded in triplicate. Relative mRNA expression levels were determined via the $2^{-\Delta\Delta CT}$ method or log-transformed.

Tissue homogenization and western blot analysis: Isolated colon tissue sections (1 cm) were homogenized using a Mini-Rottor (BioSpec). Tissues were

lysed in complete RIPA (Boston BioProducts) buffer for western blot analysis containing Complete Protease Inhibitor cocktail (Roche) and phosphatase inhibitor cocktail (phosSTOP, Roche). All protein lysates were quantified using a quantitative BCA protein Assay (Thermo Scientific). A total of 30 µg of protein was mixed in SDS loading dye containing 20 mg/ml DTT reducing agent, boiled for 5 min, separated by SDS-PAGE using 4-12% Bis-Tris gels (Novex) and wet transferred to nitrocellulose membrane (Roche). Nitrocellulose membranes were blocked for 1 hr with 10% non-fat milk and incubated overnight with primary antibodies, washed 5 times with TBS-T and incubated for 1-2 hrs at RT with the appropriate goat anti-rabbit or bovine anti-goat HRP conjugated secondary antibodies (Santa Cruz and Sigma Aldrich). Protein expression was determined using the following antibodies: phospho-IκBα (Cell Signaling), IκBα (Santa Cruz), phospho-p65 (Cell Signaling), p65 (Cell Signaling), phospho-ERK1/2 (Cell Signaling), ERK1/2 (Santa Cruz), phospho-JNK1/2 (Cell Signaling), JNK1/2 (Santa Cruz), phospho-STAT3 (Cell Signaling), STAT3 (Cell Signaling) and Actin (Santa Cruz).

Isolation of colon crypts: Following a previously described protocol (Fuller et al., 2013), colons were removed and flushed with cold PBS. Colons were cut into 2-3 cm pieces and transferred to 3mM EDTA/1.5mM DTT in PBS and place on ice for 30 minutes. After manual shaking for 30 seconds, the tissue is moved to fresh cold PBS with 3 mM EDTA and placed at 37°C for 10 minutes. Samples were shaken vigorously for 1 minute to separate the colon crypts from the

submucosa. The submucosa was discarded, the samples were spun at 300 x g for 5 minutes and the pellet was frozen for protein preparation.

Flow cytometric analysis of colon crypt cells. Colon crypt cells were collected and washed with PBS, re-suspended in FACS staining buffer (PBS supplemented with 5% fetal bovine serum) and counted. A total of 10^7 cells/mL were stained with both CD45-FITC (BD Bioscience) and EpCAM-APC (BD Bioscience) in FACS staining buffer. Flow cytometry was performed using an LSRII (BD Biosciences), and the resulting data was analyzed using FlowJo (TreeStar).

Colon tissue explants for the analysis of cytokine production: Colon cytokine secretion was assessed by flushing colons with PBS containing penicillin/streptomycin. The distal-most 1-cm^2 colon sections were cultured for 15 h in RPMI media containing penicillin/streptomycin. Supernatants from these cultures were removed, cleared of debris by centrifugation and assessed for mouse cytokines by ELISA (BD Biosciences).

Anti-IL-6R Antibody Treatment of Mice: IL-6 blockade was achieved using an intraperitoneal injection of 20 μg/mL of Tocilizumab (Genentech) every two weeks for 10 weeks. Animals of 6 weeks of age were monitored weekly for weight changed and body condition after initiation of antibody treatment.

Bioinformatics analysis of *NLRX1* expression in human CRC: Microarray studies containing data that focused on the expression of *NLRX1* in CRC were

obtained using the gene search function of the Oncomine® Platform (www.oncomine.org). The default parameters set by the platform were used: threshold fold change was greater or equal to 1.5X, *p* value was greater or equal to 0.0001 and the gene rank was in the top 10%. Data analysis was expressed as fold change of expression in CRC compared to normal tissues (Wang et al., 2014). Data from the five CRC datasets were designated by the first author and by the numbers of patient [CRC/normal controls]: Gaedcke [65/65] (Gaedcke et al., 2010), Skrzypczak [81/24] (Skrzypczak et al., 2010), TCGA colon cancer [215/22] (Cancer Genome Atlas, 2012), Kaiser [100/5] (Kaiser et al., 2007) and Graudens [18/12] (Graudens et al., 2006). Following an analysis of *NLRX1* expression, the results from these databases were sorted based on the *p* value, and the log-transformed median centered raw data were downloaded from the Oncomine® Platform. Graph Pad software was used to create the boxplots and dot figures.

Collection of clinical CRC specimens: Bio-specimens were collected from 40 patients newly diagnosed with colon or rectum adenocarcinoma as previously described (Liu et al., 2015). These patients underwent surgical resection during 2014 at the Xijing Hospital in Xi'an, China. None of the patients in this analysis received any prior treatment including chemotherapy and/or radiotherapy. All of the samples were collected and stored in agreement with the approved protocols of Xijing Hospital. The IRB was approved by the Institutional Research Ethics Committees in Xijing Hospital, Xi'an, China. Samples that were used for our

analyses were numbered and did not include any patient identifying information that is protected under the IRB agreement.

Cases were staged according to the American Joint Committee on Cancer staging system (AJCC) (Cancer Genome Atlas, 2012). Adjacent normal tissue specimens taken at a distance that is >2 cm from the actual tumor were used as controls. Histologic sections were obtained from top and bottom portions of each formalin-fixed and paraffin embedded (FFPE) specimen. Each tumor specimen weighed between 60 and 200 mg. Normal and cancerous sample were stained with H&E and examined by two board-certified pathologists (P.H. and Z.L.) to confirm the presence of CRC in the specimens. The pathologists confirmed that each tumor sample was histologically consistent with colon adenocarcinoma and that tumor cells were not present in the adjacent normal specimen (Cancer Genome Atlas, 2012).

RNA extraction from FFPE tissues and quantitative real-time PCR: RecoverAll™ Total Nucleic Acid Isolation Kit was used to isolate RNA from FFPE tissues according to the manufacturer's protocol (AM1975, Ambion Austin, TX). Briefly, 1 ml of 100% xylene was added to 3 pieces of 20 mm thick FFPE sections. Samples were incubated for 3 min at 50°C to remove traces of paraffin and centrifuged for 2 min to remove the xylene. Pellets were washed twice with 1 ml of 100% ethanol, digested with 200 µl of proteinase K digestive buffer at 50°C overnight and then incubated with DNase I. Samples were washed, total RNA was eluted with distilled water and the RNA concentration of each sample was

determined by a Nanodrop 2000 spectrophotometer. IScript™ cDNA Synthesis Kit was used to generate cDNA and Q-PCR was performed for human *NLRX1* (Hs00226360_m1), *GAPDH* (Hs02758991_g1), *ACTB* (Hs01060665_g1) and *18S rRNA* (Hs03928985_g1). All samples were analyzed in triplicate. Relative mRNA expression levels were determined by the $2^{-\Delta\Delta CT}$ or log-transformed method.

Statistics for Clinical Human Samples: For the analysis of clinical human samples, ratios of real-time PCR values of case-matched normal and CRC tissues were determined. Normalization was performed by determining the mean expression value of three internal control genes: *ACTB*, *GAPDH* and *18S rRNA*. Differences between two sample groups were analyzed using the paired or unpaired Student's t-test (Mann–Whitney unpaired test or Wilcoxon matched-pairs signed test). The association between gene expression levels and clinical parameters was performed by the analysis of variance (ANOVA). A *p* value that is <0.05 is considered statistically significant. All statistical analysis was performed using the Graph pad Prism software.

SUPPLEMENTAL REFERENCES

Allen, I.C., TeKippe, E.M., Woodford, R.M., Uronis, J.M., Holl, E.K., Rogers, A.B., Herfarth, H.H., Jobin, C., and Ting, J.P. (2010). The NLRP3 inflammasome functions as a negative regulator of tumorigenesis during colitis-associated cancer. The Journal of experimental medicine *207*, 1045-1056.

Cancer Genome Atlas, N. (2012). Comprehensive molecular characterization of human colon and rectal cancer. Nature *487*, 330-337.

Ding, S., Blue, R.E., Morgan, D.R., and Lund, P.K. (2014). Comparison of multiple enzyme activatable near-infrared fluorescent molecular probes for detection and quantification of inflammation in murine colitis models. Inflammatory bowel diseases *20*, 363-377.

Ding, S., Eric Blue, R., Chen, Y., Scull, B., Kay Lund, P., and Morgan, D. (2012). Molecular imaging of gastric neoplasia with near-infrared fluorescent activatable probes. Molecular imaging *11*, 507-515.

Fuller, M.K., Faulk, D.M., Sundaram, N., Mahe, M.M., Stout, K.M., von Furstenberg, R.J., Smith, B.J., McNaughton, K.K., Shroyer, N.F., Helmrath, M.A., and Henning, S.J. (2013). Intestinal stem cells remain viable after prolonged tissue storage. Cell Tissue Res *354*, 441-450.

Gaedcke, J., Grade, M., Jung, K., Camps, J., Jo, P., Emons, G., Gehoff, A., Sax, U., Schirmer, M., Becker, H.*, et al.* (2010). Mutated KRAS results in overexpression of DUSP4, a MAP-kinase phosphatase, and SMYD3, a histone methyltransferase, in rectal carcinomas. Genes, chromosomes & cancer *49*, 1024-1034.

Graudens, E., Boulanger, V., Mollard, C., Mariage-Samson, R., Barlet, X., Gremy, G., Couillault, C., Lajemi, M., Piatier-Tonneau, D., Zaborski, P.*, et al.* (2006). Deciphering cellular states of innate tumor drug responses. Genome biology *7*, R19.

Jaffer, F.A., Vinegoni, C., John, M.C., Aikawa, E., Gold, H.K., Finn, A.V., Ntziachristos, V., Libby, P., and Weissleder, R. (2008). Real-time catheter molecular sensing of inflammation in proteolytically active atherosclerosis. Circulation *118*, 1802-1809.

Kaiser, S., Park, Y.K., Franklin, J.L., Halberg, R.B., Yu, M., Jessen, W.J., Freudenberg, J., Chen, X., Haigis, K., Jegga, A.G.*, et al.* (2007). Transcriptional recapitulation and subversion of embryonic colon development by mouse colon tumor models and human colon cancer. Genome biology *8*, R131.

Liu, R., Truax, A.D., Chen, L., Hu, P., Li, Z., Chen, J., Song, C., Chen, L., and Ting, J.P. (2015). Expression profile of innate immune receptors, NLRs and AIM2, in human colorectal cancer: correlation with cancer stages and inflammasome components. Oncotarget *6*, 33456-33469.

Meira, L.B., Bugni, J.M., Green, S.L., Lee, C.-W., Pang, B., Borenshtein, D., Rickman, B.H., Rogers, A.B., Moroski-Erkul, C.A., McFaline, J.L.*, et al.* (2008). DNA damage induced by chronic inflammation contributes to colon carcinogenesis in mice. The Journal of clinical investigation *118*, 2516-2525.

Neufert, C., Becker, C., and Neurath, M.F. (2007). An inducible mouse model of colon carcinogenesis for the analysis of sporadic and inflammation-driven tumor progression. Nature protocols *2*, 1998-2004.

Skrzypczak, M., Goryca, K., Rubel, T., Paziewska, A., Mikula, M., Jarosz, D., Pachlewski, J., Oledzki, J., and Ostrowski, J. (2010). Modeling oncogenic signaling in colon tumors by multidirectional analyses of microarray data directed for maximization of analytical reliability. PLoS One *5*.

Uronis, J.M., Mühlbauer, M., Herfarth, H.H., Rubinas, T.C., Jones, G.S., and Jobin, C. (2009). Modulation of the Intestinal Microbiota Alters Colitis-Associated Colorectal Cancer Susceptibility. PLoS ONE *4*, e6026.

Wang, L., Yao, Z.Q., Moorman, J.P., Xu, Y., and Ning, S. (2014). Gene expression profiling identifies IRF4-associated molecular signatures in hematological malignancies. PLoS One *9*, e106788.

Zhang, H., Morgan, D., Cecil, G., Burkholder, A., Ramocki, N., Scull, B., and Lund, P.K. (2008). Biochromoendoscopy: molecular imaging with capsule endoscopy for detection of adenomas of the GI tract. Gastrointestinal endoscopy *68*, 520-527.